Near Wall Reaction Effects on Film-Cooled Backward-Facing Step Heat Transfer
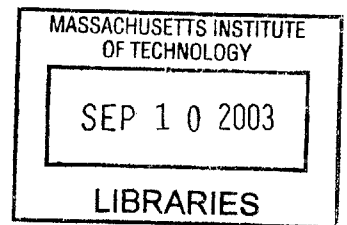
by

David Wade Milanes

B.S. Mechanical Engineering
Louisiana State University, 2001

Submitted to the Department of Aeronautics and Astronautics
in partial fulfillment of the requirements for the degree of

Master of Science in Aeronautics and Astronautics

at the

Massachusetts Institute of Technology
June 2003

Author: _____

David Wade Milanes
Department of Aeronautics and Astronautics
May 23, 2003

Certified by: _____

Ian A. Waitz
Professor and Deputy Head, Aeronautics and Astronautics
Thesis Supervisor

Accepted by: _____

Edward M. Greitzer
Professor of Aeronautics and Astronautics
Chairman, Departmental Graduate Committee

AERO

Near Wall Reaction Effects on Film-Cooled Backward-Facing Step Heat Transfer

by

David W. Milanes

Submitted to the Department of Aeronautics and Astronautics
on May 23, 2003, in partial fulfillment of the
requirements for the degree of
Master of Science in Aerospace Engineering

Abstract

As specific thrust requirements for aircraft gas turbine engines increase, higher fuel-air ratios will be be employed in the combustor. As the fuel-to-air ratio increases, so does the potential for partially-reacted gas mixtures to leave the combustor and react with filmcooling flows in the turbine. One area for particular concern are locations where abrupt steps in the endwall produce recirculation zones. Due to the high residence times characteristic of recirculation zones, there is an increased likelihood for residual energetic species emitted from the combustor to react with turbine film-cooling air. However, there is currently little understanding of the mechanisms that govern heat flux augmentation due to reactions downstream of film-cooled backward-facing step geometries.

A set of non-dimensional parameters that governs reacting film cooled backward-facing step heat transfer is presented. These include the scaled heat flux Q_s, the Damköhler number Da, the heat release potential H^*, and the mass blowing ratio B. A shock tunnel experiment was employed to generate short duration, high temperature (1000-2800 K) and pressure (6 atm.) fuel-rich flows over a film-cooled backward-facing step. The relative increase in surface heat flux due to near-wall reactions was investigated over a range of the subset of governing parameters. Experimental measurements showed that up to 75% of the theoretical maximum possible heat flux augmentation could be achieved. A reduced-order analytical model was developed to predict the heat flux augmentation due to reactions downstream of the backward-facing step. Assuming that the cooling jet did not affect the recirculation zone flow structure and the recirculation zone was "well-mixed", a perfectly stirred reactor model showed that up to 30% of the theoretical maximum possible heat flux augmentation could be achieved. The differences between the heat flux augmentation predicted by the model and the values measured with experiments were noted and attributed to the alteration of the recirculation zone flow structure by the cooling jets in the experiments.

Thesis Supervisor: Ian A. Waitz
Title: Professor and Deputy Head, Department of Aeronautics and Astronautics

Acknowledgements

I would like to express my deepest gratitude to Professor Ian Waitz. Your constant encouragement and profound insight kept me going throughout this project.

I would also especially like to thank Dr. Dan Kirk and Steve Lukachko. Both of you were invaluable in getting me started on this project, and keeping me going through the experiments and modeling.

I would like to thank Dr. Gerald Guenette for his help with MATLAB codes and temperature gage calibration. Thanks to Professors Ed Greitzer and Frank Marble for their insightful and penetrating questions posed during presentations of this work. Jack Costa, Jimmy Letendre, Viktor Dubrowski, and Bill Ames, I thank all of you for your assistance with machining, assembly, order, and experimental troubleshooting.

Thanks to the Aero/Astro department here at MIT. For two years, I have received support from this department, which has been essential to this work.

There are so many people that I have met here at MIT that have helped get me through these last two years. Dan, Vikas, Chris, CP, Mark, Nick, John, Dennis, Steve, Shana, Neil, Benny, Jay, Sajjad, Siddharth, Jameel, and Andy, you guys have all helped to make my MIT experience fun and life-changing. Indeed, your peers are truly the best source of information you have while at MIT.

To my family—Mom, Dad, Andrew, Katie, Nick, Brady, Caroline, and Spencer—I dedicate this work. You have inspired me never to settle for less than my personal best, which I think is the single greatest lesson I have ever learned in life.

Finally, I would like to dedicate this work to my love, Arely. During the last year and a half, I've had the best times of my life with you. You have challenged me to learn more about myself than anyone else ever has. Thank you for being in my life.

Table of Contents

List of Figures

11

List of Tables

Nomenclature

Roman

A	boundary surface area
B	mass blowing ratio
c_p	specific heat at constant pressure
D	cooling hole diameter
D^*	normalized step height
Da	Damköhler number
ER	expansion ratio
I	momentum blowing ratio
h	convection coefficient
H	enthalpy or step height
H^*	heat release potential
L_c	distance from step face to cooling hole
$\dot{m}$	mass flow rate
$\dot{n}$	molar flow rate
P	pressure
q	heat flux
$\dot{Q}$	heat transfer rate
Q_s	scaled heat flux
r	reaction rate
Re	Reynolds number
T	temperature
u	streamwise velocity
V	reactor volume
W	channel height

Greek

δ	boundary layer thickness
δ_H^*	normalized boundary layer thickness
ν	kinematic viscosity
ρ	fluid density
τ	characteristic time scale

Subscripts

1	duct upstream of step
2	duct downstream of step
c	cooling jet
chem.	time scale to achieve 95% maximum possible temperature change
cold	non-reacting conditions
e	entrained flow from mixing layer
flow	flow convection time scale
hot	reacting conditions
∞	freestream conditions
max	theoretical maximum possible reacting conditions
t	stagnation conditions
wall	wall boundary conditions

Superscripts

j	j-th molar species

Chapter 1

1 Introduction

1.1 Background

As specific thrust requirements of aircraft engines increase, higher turbine inlet temperatures will be employed. Higher fuel-air ratios, therefore, will be needed to meet future aircraft performance requirements. This leads to a potential problem, depicted in Figure 1-1, in which residual fuel present in the freestream could react with turbine film-cooling flows. These reactions would be promoted by the high fluid residence times that characterize the recirculation region behind backward-facing steps, such as the lip of a turbine endwall.
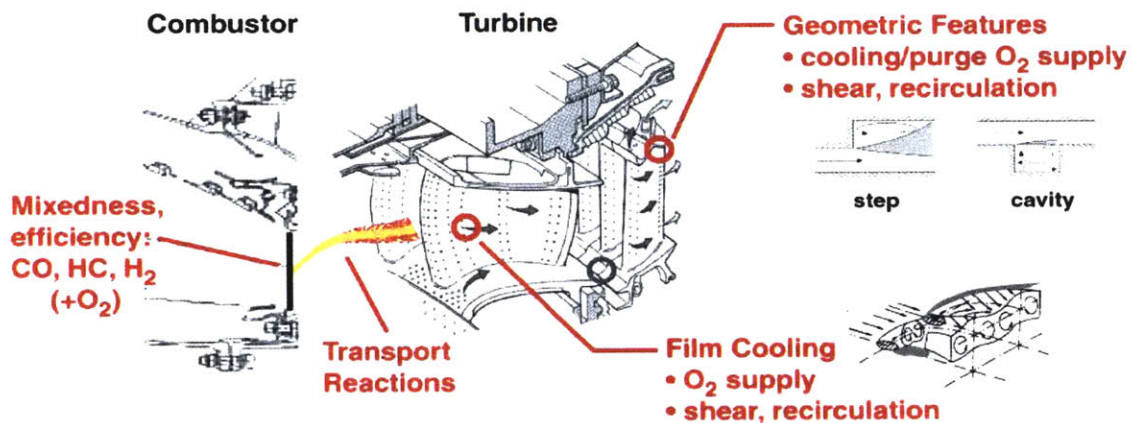
Figure 1-1: High fuel-air ratio problem

This high fuel-air ratio (HFA) phenomenon can be divided into three phases:

1) exhaust of energetic species from the combustor
2) migration of the energetic species downstream into the turbine
3) mixing of the energetic species with turbine film-cooling flows.

1.1.1 Phase One: Species Exhaust

Increasing fuel-air ratios can lead to energetic species exiting the combustor as shown by Lukachko, et al. [1]. Both incomplete mixing and insufficient time to

17

complete reactions can lead to the exhaust of lower molecular weight hydrocarbon species. The higher temperatures associated with high fuel-air ratios facilitate the production of reactive dissociation products, such as CO and OH (even under conditions of thermodynamic equilibrium and complete mixing). All of these reactive species are potential by-products of HFA combustion and fuel for possible downstream reactions.

1.1.2 Phase Two: Downstream Migration

After exhaust from the combustor, the species migrate through the turbine. During this migration, the reactive species continue to mix with the oxidizer also present in the freestream. As the reactive species and oxidizer mix, chemical reactions are initiated. Lukachko, et al. [1] found the characteristic width of the reactive species streak to be an important parameter governing the degree to which chemical reactions are completed during the migration period between the combustor and the turbine. Reactive streaks exiting the combustor with widths greater than 10-20% of the radial passage height are large enough to prevent full mixing and reaction before the streak reaches the turbine.

1.1.3 Phase Three: Near-wall Mixing

As reactive streaks pass through the turbine, mixing between the fuel-rich streaks and oxidizer-rich turbine film-cooling flows can occur. Given the right turbine fluid dynamic and thermodynamic conditions, the time required for chemical reactions to complete may be less than the length of time during which the fuel and oxidizer streaks are in contact. Thus, the possibility of near-wall chemical reactions arises leading to elevated heat flux to turbine components.

What turbine conditions could promote such reactions? High freestream pressure and temperature increase the chemical reaction rate, and therefore lower the characteristic chemical reaction time, which increases the potential for reactions. If the length of time during which the fuel and oxidizer streaks are in contact is extended, then chemical reactions are promoted. As detailed in the

18

next chapter of this thesis, the recirculation zone behind the face of a backward-facing step is characterized by high fluid residence times. These high fluid residence times provide an increased contact time for any fuel and oxidizer streaks that enter the recirculation zone. Thus, the presence of a backward-facing step could promote fuel and oxidizer streak chemical reactions.

1.2 Review of Previous Research

Much work has been done in previous high fuel-air ratio studies to characterize the potential for elevated heat flux due to near-wall chemical reactions. Kirk [2] performed short-duration heat flux experiments on a reacting film-cooled flat plate. A governing set of non-dimensional parameters was developed for reacting film-cooled flat plate flow. Surface heat flux augmentation up to 80% of a theoretical thermodynamic maximum value was measured for realistic non-dimensional engine conditions. Lukachko, et al. [1], as mentioned in the previous section, modeled combustor exhaust energy content levels. Exhausts with the energetic equivalent of up to 40,000-60,000 ppm CO were predicted for combustors with combustion efficiency and mixedness level deficiencies. Reactive streaks exiting the combustor with widths greater than 10-20% of the radial passage height were predicted to be large enough to prevent full mixing and chemical reaction before the streak reaches the turbine.

The previous high fuel-air ratio studies done by Kirk, and Lukachko, et al. focused on the freestream and near-wall reactions on film-cooled flat plates, the latter as a model for film-cooled airfoil surfaces. However, other geometries commonly found in aircraft engines, such as backward-facing steps, potentially could promote more complete chemical reactions than were measured over the film-cooled flat plate. Due to the high fluid residence times characteristic of recirculating flows, fuel and oxidizer are more likely to mix and react if entrained into the recirculating region downstream of a backward-facing step. If combustion were sustained in the recirculation region downstream of a backward-facing step, then higher surface heat flux could result.

The backward-facing step is a simple geometry that has been extensively studied in the field of thermofluids. Each study lacks at least one of the main elements that characterize the problem studied in this thesis: film-cooling flow downstream of step, presence of fuel in freestream, and mixing of fuel and oxidizer streams.

Both the flow structure and the heat transfer profile of a backward-facing step without film-cooling and residual fuel have been studied. Adams, Johnson and Eaton [3] identified a set of non-dimensional parameters governing the fluid dynamics and heat transfer of un-cooled, non-reacting backward-facing step flow. Aung and Goldstein [4] characterize the recirculation zone—the region of fluid immediately downstream of the step face—as a region of low momentum fluid with backflow and entrainment exchange with the separating flow. The reattachment point—the location at which the flow separated over the step lip reattaches to the wall—is found to be approximately 6-8 step heights downstream of the step face, Aung and Goldstein [4], Seban, et al. [5]. Vogel and Eaton [6] note that the reattachment point also corresponds to the location of the maximum Stanton number in the recirculation zone.

The structure of the recirculation zone behind a backward-facing step with injection in the recirculation zone was studied by Harinaldi, Ueda, and Mizomoto [7]. Blowing jets with varying velocity ratio relative to the freestream value were studied at two different locations downstream of the step face. Downstream injection location was shown to affect the extent to which the recirculation zone flow structure was altered by flow injection. For flow injection of the same velocity ratio located at two different locations downstream of the step face, the injection closer to the step face was shown to alter the recirculation zone structure more strongly. Increasing blowing-to-freestream velocity ratios also produced stronger alterations to the recirculation zone flow structure.

The reaction of premixed fuel and oxidizer in the wake of bluff bodies has been studied by Zukoski and Marble [8]. Experiments revealed that hot streaks were entrained into the wake of bluff bodies. The recirculation zone behind the

bluff body became filled with hot gases that were entrained by the passing flow. As a premixed fuel and oxidizer mixture passed the wake of the bluff body, these hot gases were entrained and promoted chemical reactions. Chemical reactions could be sustained when the flow time past the wake was long enough to allow chemical reactions to proceed to near-completion thereby replenishing the wake of hot gases with reaction products. Though the present thesis deals with non-premixed combustion, the Zukoski and Marble research could be used to describe the combustion processes for a specific case of reacting film-cooled step flow with infinitely fast mixing—as detailed in section 2.3.

1.3 Research Objectives

The main goal of this research is to understand heat flux augmentation behind reacting film-cooled backward-facing steps. Specifically, the following goals were established:

- Develop the set of non-dimensional parameters that govern film-cooled reacting backward-facing step heat transfer.

- Predict the maximum surface heat flux augmentation due to film-cooled backward-facing step reactions for any geometric, thermodynamic, and fluid dynamic conditions.

- Determine the minimum step height needed to support near-wall reactions for any geometric, thermodynamic, and fluid dynamic conditions.

- Show how the surface heat flux augmentation varies spatially downstream of the step face.

1.4 Research Contributions

The following are the major research contributions detailed in the present thesis:

- A set of non-dimensional parameters governing reacting film-cooled backward-facing step heat transfer is presented.

- A reduced-order perfectly-stirred reactor (PSR) model is used to predict augmented heat flux for a specific case of reacting step flow.

- The first set of experimental heat flux data for reacting step flow is presented.

- A momentum blowing ratio governing the structure of the recirculation zone in film-cooled step flow is proposed.

1.5 Thesis Overview

This chapter has introduced the phenomenon of intra-turbine heat release in high fuel-air ratio engines. It also outlined previous research on the heat transfer characteristics and fluid dynamic structure of backward-facing steps. A list of research objectives and contributions was presented.

Chapter two presents the technical approach followed to meet the research objectives. The basic concepts of flow behind backward-facing steps are presented. A set of non-dimensional parameters that governs reacting film-cooled backward-facing step heat transfer is presented. An overview of both the reduced-order analytical modeling and reacting step experiments is presented.

The reduced-order perfectly stirred reactor (PSR) model is presented in chapter three. The development of the model is discussed, and a parametric study is performed to note model predictions for various engine conditions.

Chapter four details the reacting heat transfer experiments performed on the film-cooled backward-facing steps. Measurements of dimensional and scaled heat flux data are presented for film-cooled backward-facing step geometry, and these results are compared to the reacting film-cooled flat plate geometry.

In chapter five, the predictions of the reduced-order analytical model and the results of the reacting experiments are compared. Both sets of results are used to formulate a preliminary design procedure for mitigating augmented heat flux due to reactions downstream of film-cooled backward-facing steps.

Chapter six presents the conclusions of this thesis along with recommendations for future work.

Chapter 2

2 Technical Approach

This chapter presents the technical approach used to study the heat transfer impacts of reactions behind film-cooled backward-facing steps.

The first section presents a basic overview of the fundamentals of backward-facing step flow. Flow structure and heat transfer characteristics downstream of the step face are discussed.

In section two of this chapter, the set of non-dimensional parameters that governs reacting film-cooled backward-facing step heat transfer is presented. The choice of each parameter is motivated by carefully considering the governing physics of the reacting backward-facing step problem.

Section three of this chapter introduces the reduced-order perfectly stirred reactor (PSR) model. An argument based on mixing and flow time scales is presented to justify PSR model application to a specific class of reacting film-cooled backward-facing step scenarios.

Section four of this chapter introduces the heat transfer experiments of reacting film-cooled backward-facing steps. The motivation for the experiments is presented along with what useful results are expected to be found.

2.1 Backward-facing Step Basics

Figure 2-1 shows typical backward-facing step geometry. The two flow regions of greatest interest to reacting film-cooled step heat transfer are the mixing layer and the recirculation zone. Basic details of the flow structure and heat transfer characteristics behind the backward facing step are presented in the following sub-sections.
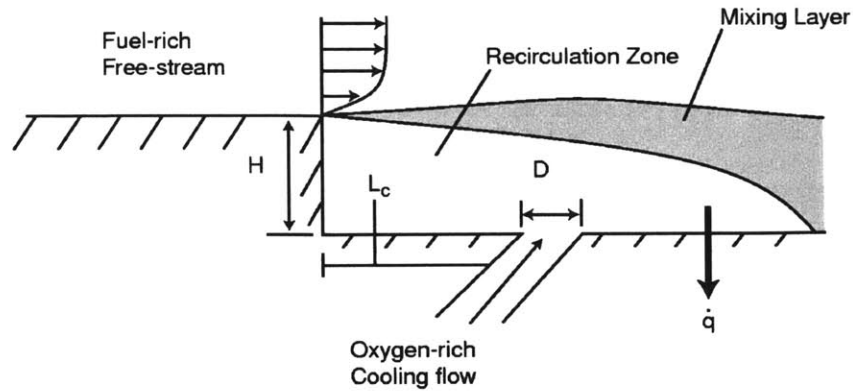
Figure 2-1: Typical film-cooled backward-facing step geometry

2.1.1 Flow Structure

Adams, Johnston, and Eaton [3] identified five separate flow zones in backward-facing step flow. Due to the highly turbulent nature of backward-facing step flow, the boundaries of the flow zones are not clearly defined. The present thesis considers zones 2a and 2b to be part of a larger mixing layer zone, here called 2. Figure 2-2 shows backward-facing step geometry with approximate boundaries of the flow zones.
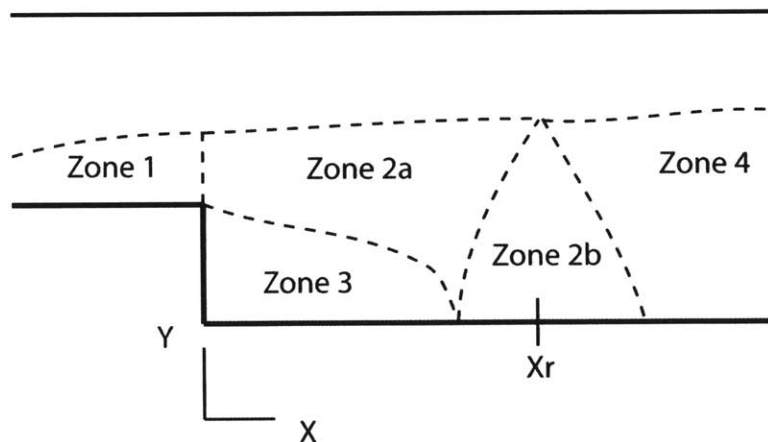
Figure 2-2: Salient flow zones for backward-facing step

2.1.1.1 Zone 1: Upstream Boundary Layer

Flow in this zone is like that in an ordinary boundary layer. The flow structure in this zone forms the initial conditions for the rest of the flow field. Bradshaw and Wong [9] postulate that the magnitude of the normalized boundary layer

24

thickness non-dimensional parameter, see section 2.2, dictates three possible flow regimes. If the normalized boundary layer thickness is much less than unity, as is the case in the experiments described in chapter 4, then the separation acts as an overwhelming boundary layer perturbation, and the free-shear layer (zone 2) structure quickly erases all traces of the upstream flow.

2.1.1.2 Zone 2: Mixing Layer

The mixing layer bounds the freestream flow region and the recirculation zone. It is characterized by strong local turbulence production which results in rapid momentum exchange and flow entrainment, Coates and Richardson [10].

Adams, Johnston, and Eaton [3] separate the mixing layer into a free shear layer and reattachment zone. Both are characterized by the convection of turbulent eddies, but the structure of the two zones is different. The free shear layer region grows under fairly constant pressure for the first 50% of the reattachment distance. Flow structure is very similar to the plane shear layer with entrainment from the recirculation zone into the free shear layer. The beginning of the reattachment region corresponds to the beginning of the adverse wall pressure gradient due to flow separation. This adverse pressure gradient can force low momentum fluid back toward the step face and into the recirculation region.

In premixed combustion in the wake of bluff bodies, and in a limiting case of non-premixed reacting film-cooled backward-facing step flow, reactions can occur in the mixing layer. These reactions are driven by the entrainment of hot gases from the recirculation zone, and sustained by the replenishment of the hot gases with reaction products.

In the present thesis, a key assumption of the reduced order model that is developed to predict heat flux augmentation due to step reactions is that chemical reactions do not occur in the mixing layer. The focus is on predicting reactions that occur within the recirculation zone.

2.1.1.3 Zone 3: Recirculation Region

The recirculation zone is perhaps the most distinct feature of backward-facing step flow. Freestream flow passes over the salient edge of the step face, separates from the wall, and then reattaches to the wall at some downstream reattachment distance. The region of flow beneath the separated flow, between the step face and the reattachment point, is characterized by low momentum, circulating fluid. In the present thesis, coolant flow is injected into the recirculation zone. Depending upon the injection location and blowing ratio, the structure of the recirculation zone can be altered as described in section 1.2.

Given the right thermodynamic and fluid dynamic conditions, combustion between oxidizer injected in the cooling flow and fuel entrained from the freestream can occur. A reduced-order analytical model, presented in section 2.3 and detailed in chapter 3, is developed to predict the surface heat flux augmentation due to combustion in the recirculation zone.

2.1.1.4 Zone 4: Recovery Zone

The wall boundary layer begins to redevelop in the recovery zone. Approximately 10 step heights after reattachment are needed for inner-layer recovery, but as many as 100 step heights are needed for the recovery of the outer-layer shear stress distribution due to large outer-layer disequilibrium.

2.1.2 Heat Transfer Characteristics

As stated by Aung and Goldstein [4], Reynolds analogy does not hold in the recirculation region of backward-facing step flow. This complicates matters somewhat by necessitating experiments or computational simulations to determine convective heat transfer coefficients downstream of backward-facing steps. Much research, such as that of Vogel and Eaton [6], shows that the convective heat transfer coefficient increases with downstream distance from the step face until a maximum is reached at the reattachment point. This value is

26

typically on the order of 1.2 times the convection coefficient value just upstream of the step face, Aung and Goldstein [4].

2.2 Non-Dimensional Parameters

The following set of non-dimensional parameters that governs reacting film-cooled backward facing step flow has been formed. A complete parameter set is derived by superposition of three sets of backward-facing step governing flow parameters. The first set, developed by Adams, Johnston, and Eaton [3], governs un-cooled, non-reacting backward facing step flow. Coolant injection effects are accounted for by adding a second set of parameters proposed by Harinaldi, Ueda, and Mizomoto [7]. Finally, effects due to near wall reactions are captured by introducing the non-dimensional parameters developed by Kirk [2]. Table 2-1 shows a summary of the non-dimensional parameters.

Table 2-1: Governing non-dimensional parameters

$\mathrm{Re}_H = \dfrac{u_\infty H}{\nu}$	Step Height Reynolds Number
$ER = \dfrac{W_2}{W_1}$	Expansion Ratio
$\delta_H^* = \dfrac{\delta}{H}$	Normalized Boundary Layer Thickness
$I = \dfrac{\rho_c u_c^2}{\rho_\infty u_\infty^2}$	Momentum Blowing Ratio
$D^* = \dfrac{H}{D}$	Normalized Step Height
$L_c^* = \dfrac{H}{L_c}$	Normalized Cooling Distance
$Q_s = \dfrac{q_{hot} - q_{cold}}{q_{max} - q_{cold}}$	Scaled Heat Flux
$Da = \dfrac{\tau_{flow}}{\tau_{chem}}$	Damköhler Number

$H^* = \dfrac{\Delta H}{H_\infty}$	Heat Release Potential
$B = \dfrac{\rho_c u_c}{\rho_\infty u_\infty}$	Mass Blowing Ratio

The physical motivation for including each parameter listed in Table 2-1 is discussed in the following sections. After discussing each parameter, a subset of parameters is defined in which experimental and analytical results are presented in chapters three and four.

2.2.1 Un-cooled non-reacting step flow dimensionless parameters

A governing set of non-dimensional parameters for un-cooled, non-reacting conditions are described by Adams, Johnston, and Eaton [3]. The global flow regime—laminar or turbulent—and the following three parameters were found to completely describe backward-facing step flow.

2.2.1.1 Step Height Reynolds Number, Re$_H$

Steady fluid flow over a backward-facing step is governed by the forces described by the two-dimensional, incompressible, Navier-Stokes equations with appropriate boundary conditions.

$$\mathbf{u} \cdot \nabla \mathbf{u} = \frac{\nabla p}{\rho} + \nu \nabla^2 \mathbf{u} \qquad \text{2-1}$$

If the freestream velocity and step height are chosen for reference velocity and length scales, then the Navier-Stokes equations can be non-dimensionalized into the following form:

$$\tilde{\mathbf{u}} \cdot \nabla \tilde{\mathbf{u}} = \nabla \tilde{p} + \frac{1}{\mathrm{Re}_H} \nabla^2 \tilde{\mathbf{u}} \qquad \text{2-2}$$

where

$$\mathrm{Re}_H = \frac{u_\infty H}{\nu} \qquad \text{2-3}$$

As seen by equation 2.3, the Reynolds number based on freestream velocity and step height is an important non-dimensional parameter describing the physics of backward-facing step flow.

2.2.1.2 Expansion Ratio, ER

The geometry of the backward-facing step leads to the second non-dimensional parameter—the expansion ratio, ER.

$$ER = \frac{W_2}{W_1} \qquad\qquad 2\text{-}4$$

This parameter measures the non-dimensional magnitude of the step expansion.

2.2.1.3 Normalized Boundary Layer Thickness, δ_H^*

Boundary conditions are necessary to constrain the governing Navier-Stokes equations. The boundary conditions are set by specifying an inlet velocity profile—described non-dimensionally as the normalized boundary layer thickness.

$$\delta_H^* = \frac{\delta}{H} \qquad\qquad 2\text{-}5$$

This parameter measures the ratio of the boundary layer thickness at the step corner relative to the step height.

2.2.2 Film-cooled non-reacting step flow parameters

The first two of the following parameters were proposed by Harinaldi, Ueda, and Mizomoto [7] to characterize the effects of blowing on the flow structure of the recirculation zone. The final parameter is presently proposed to account for the effects of different sized cooling holes.

2.2.2.1 Momentum blowing ratio, I

The first important parameter presented by Harinaldi, Ueda, and Mizimoto is the momentum blowing ratio, I. This ratio is typically written in the following manner:

$$I = \frac{\rho_c u_c^2}{\rho_\infty u_\infty^2}$$
2-6

Momentum blowing ratio measures the ratio of coolant flow momentum flux relative to freestream flow mass flux, and is typically used when studies of the cooling jet structure are performed.

2.2.2.2 Normalized Step Height, D^*

Adding the backward-facing step to the film-cooled flat plate adds two length scale ratios. The first is the normalized step height, D^*:

$$D^* = \frac{H}{D}$$
2-7

This parameter measures the ratio of the step height relative to the cooling hole diameter. While this parameter was not explicitly proposed by Harinaldi, Ueda, and Mizomoto—likely because only one particular step height and cooling slot was investigated in their experiments—it is plausible to expect the relative size of the cooling hole to affect the structure of the recirculation zone.

2.2.2.3 Normalized Cooling Distance, L_c^*

The second additional length scale ratio is the normalized cooling distance, L_c^*:

$$L_c^* = \frac{H}{L_c}$$
2-8

This parameter measures the ratio of the step height relative to the distance from the step face to the cooling hole.

2.2.3 Film-cooled reacting flat plate parameters

Kirk [2] proposed a set of non-dimensional parameters that govern reacting film-cooled flat plate heat transfer. A dependent dimensionless parameter, the scaled

heat flux, describes the surface heat flux augmentation due to chemical reactions. Kirk determined that the scaled heat flux is a function of other dimensionless parameters including mass blowing ratio, heat release potential, and Damköhler number.

2.2.3.1 Scaled Heat Flux, Q_s

This dependent dimensionless parameter measures the augmented wall heat flux due to chemical reactions. The scaled heat flux is written as

$$Q_s = \frac{q_{hot} - q_{cold}}{q_{max} - q_{cold}}, \qquad\qquad 2\text{-}9$$

where

q_{max} is the maximum possible heat flux to the wall—achieved when the reaction proceeds until the adiabatic flame temperature is reached.

This definition of scaled heat flux is a measure of how much surface heat flux augmentation is achieved compared to the maximum possible heat flux augmentation. The scaled heat flux can range from 0%—if $q_{hot}=q_{cold}$ and no reactions occur—to 100%—if $q_{hot}=q_{max}$ and the reaction proceeds until the adiabatic flame temperature is achieved.

2.2.3.2 Damköhler Number, Da

The Damköhler number compares the ratio of characteristic flow time scales to chemical time scales, and can be written as the following:

$$Da = \frac{\tau_{flow}}{\tau_{chem}} = \frac{L/u_{fs}}{\tau_{chem}} = \frac{X_r / M\sqrt{\gamma RT_\infty}}{\tau_{chem}}. \qquad\qquad 2\text{-}10$$

If this ratio is larger than unity, then there is enough time in the flow traverse to permit chemical reactions. When Da is less than unity, chemical reactions will not have enough time to occur during the flow traverse. The characteristic length scale is selected to be the step reattachment distance—typically 6 to 8 step heights downstream of the step face for backward-facing step flow—was chosen

31

because the reattachment distance is a key length scale over which reactions in the recirculation zone could take place.

2.2.3.3 Heat Release Potential, H*

The energy content of the freestream flow is measured by the heat release potential. Energy content levels are typically measured in equivalent ppm of CO, but the following definition for H* provides a more universal unit for fuel level:

$$H^* = \frac{\Delta H}{H_{t\infty}} \approx \frac{T_{ad} - T_{t\infty}}{T_{t\infty}} .$$

2-11

Thus, H* is the ratio of the potential increase in enthalpy of the freestream due to reaction relative to the freestream enthalpy. If Cp is constant, then H* can be approximately expressed as the ratio of the maximum possible total temperature change relative to the freestream total temperature. As noted in section 2.2.1, the maximum possible temperature change due to chemical reaction occurs when the reaction proceeds until the adiabatic flame temperature is achieved.

2.2.3.4 Mass Blowing Ratio, B

The mass blowing ratio is a common parameter used to describe film-cooling jets. Typically, the mass blowing ratio is written in the following manner:

$$B = \frac{\rho_c u_c}{\rho_\infty u_\infty} .$$

2-12

Mass blowing ratio measures the ratio of coolant flow mass flux relative to freestream flow mass flux. The mass blowing ratio is used when heat transfer studies are performed (because the Stanton number scales with mass flux).

Kirk [2] also noted that momentum blowing ratio, I, is an important parameter in characterizing the structure of the film cooling jet. The momentum blowing ratio dictates whether the cooling jet is attached to or lifted from the surface, which defines to dominant structural regimes for near-wall film-cooled reactions.

32

2.3 Reduced-order Modeling

A reduced-order analytical model was developed to predict heat flux augmentation due to reactions downstream of the backward-facing step. Reduced-order modeling provides unique challenges and opportunities. A modeler must carefully choose what level of model fidelity is prudent; a tradeoff between model simplicity and prediction accuracy is inherent. In the present thesis, modeling a specific case of reacting step flow with the simple, canonical model was the chosen approach. A simple model would facilitate parametric studies of the relevant non-dimensional space, and would be an extremely useful design tool if properly validated against higher fidelity predictions or experiments.

Five possible cases for non-premixed near wall reactions behind backward-facing steps have been identified, as adapted from Coates and Richardson [10]:

1. At very low blowing ratios, the oxidizer rich coolant flow is in sufficiently short supply that combustion should occur in close proximity to the injection site in a diffusion flame type manner.

2. As the blowing ratio is increased, stable combustion is established in the recirculation zone.

3. With a further increase of blowing ratio, the recirculation zone becomes too lean to sustain combustion and the mixing layer becomes the site of combustion activity.

4. As the blowing ratio is further increased, the cooling jet penetrates through the low momentum recirculation zone, but does not have sufficient momentum to pierce through the higher-momentum mixing layer. This results in the cooling jet bending back toward the wall and touching down at some X/D distance downstream from its injection. Combustion activity can occur in either the recirculation zone, upstream of jet injection, or mixing layer and in the near jet region.

5. In the very high blowing ratio limit, the cooling jet has sufficient momentum to pierce through both the recirculation zone and the mixing layer. No jet touchdown within the measurable X/D range is expected. Like case (4), combustion activity is expected to occur in the recirculation zone, mixing layer, or in the near jet region.

A reduced order model is developed to predict augmented heat flux conditions in case (2). Therefore, it is important to define the conditions under which case (2) is realized. The following three conditions are necessary for case (2) to exist are briefly presented to set the stage for the cases that will be modeled. Additional details of the following conditions are presented in chapter three of the present work.

1. The momentum blow ratio of the cooling jet, I, must be small enough that the structure of the recirculation zone is not affected.

2. The mixing time scale within the recirculation zone must be much less than the characteristic fluid residence time in the recirculation zone.

3. Local recirculation zone equivalence ratio must be in the range that permits combustion.

If conditions 1 and 2 are satisfied, then the recirculation zone can be modeled as a simple well-mixed zone with typical recirculation zone structure. A model widely used to predict combustion in such zones is the perfectly-stirred reactor (PSR) model. The augmented heat flux to the wall in such reactors can be predicted if the conditions into the reactor are known.

2.4 Reacting Step Experiments

A set of reacting film-cooling backward-facing step experiments were performed to measure heat flux downstream of the step face. The purpose of these experiments is threefold:

- To obtain the first set of reacting film-cooled step heat flux data.

- To compare with and possibly validate reduced-order model predictions.

34

- To elucidate governing physics of the problem that can be seen from the downstream spatial trend of the surface heat flux.

The experimental test plate used by Kirk [2] was modified by attaching a step piece upstream of the film-cooling holes. Using the MIT Gas Turbine Lab shock tunnel facility, direct heat flux measurements were collected downstream of the step face for various non-dimensional test conditions. These experiments, as detailed in chapter four, provided a wealth of heat flux information, but they failed to be an effective validation for model predictions. As described in chapter five, the discrepancy in heat flux values could be due to a different flow case being tested than was assumed in the model. Upon detailed analysis of the test data, it is believed that the tests involved flow cases 4 and 5 of section 2.3.

2.4.1 Experimental non-dimensional parameter subset

Due to the design of the experiment, it can be shown that some of the non-dimensional parameters are redundant. This simplifies the non-dimensional analysis by reducing the number of parameters needed to compare experimental runs to a smaller subset of the original ten.

The step-height Reynolds number is a function of step height, thermodynamic properties, and freestream velocity. The step height remained constant throughout the experiments. Thermodynamic properties are only functions of temperature for ideal gases, which is captured in the Damköhler number. Because the freestream Mach number is constant, the velocity is also controlled by the freestream temperature. Thus, for the experiments detailed in the present thesis, matching Damköhler number necessarily matches step-height Reynolds number.

In the experiments, the same test chamber and step piece were used for all runs. Expansion ratio, normalized cooling length, and normalized step height were, therefore, kept constant for all backward-facing step runs.

The normalized boundary layer thickness is a function of step height and streamwise Reynolds number based on the distance from the step piece leading

edge to the step face. Because the same step piece was used for all test runs, both length scales remained constant. Again, matching the Damköhler number necessarily matches the other terms in the streamwise Reynolds number.

Momentum blowing ratio is a function of mass blowing ratio and the temperature ratio of the coolant flow relative to the freestream flow. Throughout the experiments, the same coolant temperature was used, so matching the Damköhler number and mass blowing ratio necessarily matched the momentum blowing ratio.

By validating the redundancy of the above parameters in the reacting experiments, results can be presented in terms of the subset of dimensionless parameters. Conclusions from the experiments can therefore focus on the heat flux augmentation effects of changing H^*, Da, and B, which follows the form of Kirk's results [2].

2.5 Chapter Summary

This chapter presented the technical approach used to study the heat transfer impacts of reactions behind film-cooled backward-facing steps. A basic overview of the fundamentals of backward-facing step flow was presented.

The set of non-dimensional parameters that governs reacting film-cooled backward-facing step heat transfer was presented. The choice of scaled heat flux, Damköhler number, heat release potential, mass blowing ratio, normalized step height, and normalized cooling distance is motivated by physical reasons. These parameters are shown to include the governing set of non-dimensional parameters typically associated with non-reacting uncooled backward-facing step flow.

Section three of this chapter introduced the reduced-order perfectly stirred reactor (PSR) model. Five potential flow regimes are postulated, and the PSR model is presented to predict heat flux augmentation in one of the flow regimes.

Section four of this chapter introduced the heat transfer experiments of reacting film-cooled backward-facing steps. The motivation for the experiments was presented along with what useful results were expected to be found.

Chapter 3

3 Analytical Modeling

This chapter presents the analytical modeling used to predict the heat flux augmentation due to reactions behind film-cooled backward-facing steps. The first section presents the perfectly-stirred reactor (PSR) model applied to a specific subset of potential reacting film-cooled step problems. In section two, a parametric study is performed to show predicted values of scaled heat flux for a variety of non-dimensional conditions. Section three analyses these predictions to gain insight into the physics of heat transfer downstream of reacting film-cooling step flow.

3.1 PSR model

In this section the PSR model is presented. Justification for the use of the PSR model is presented for a specific case of reacting film-cooling step flow. Then, the PSR model is developed for the film-cooled backward-facing step.

3.1.1 PSR Overview

The PSR model is often used in combustion modeling to describe reactions in regions of high localized mixing. Spatial non-uniformities are neglected due to high mixing, and the reactor is characterized by a fluid with homogeneous chemical composition and thermodynamic state. Any fluid exiting the reactor, therefore, has exactly the same chemical composition and thermodynamic state as the fluid within the reactor.

$P, V, \dot{Q}$

$\dot{m}, T_{in}, \dot{n}_{in}^{j}$

$\dot{m}, T_{out}, \dot{n}_{out}^{j}$
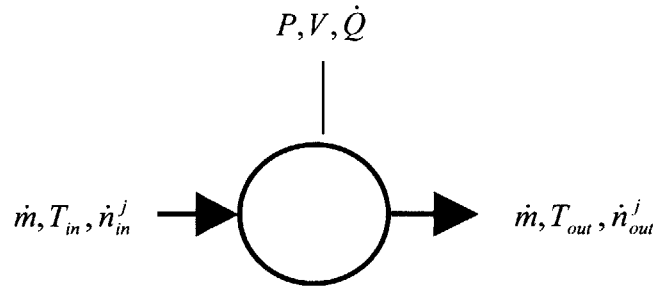
Figure 3-1: General PSR schematic

Figure 3-1 shows a generic reactor with inlet and outlet flows. Applying the conservation of mass, conservation of energy, and the general mole balance (for each molar species) yields a set of equations that describe the physics of the reactor.

$$\frac{dm_r}{dt} = \dot{m}_{in} - \dot{m}_{out}$$

3-1

$$\frac{dU_r}{dt} = \dot{Q} + \dot{m}_{in} h_{t,in} - \dot{m}_{out} h_{t,out}$$

3-2

$$\frac{dN_r^{j}}{dt} = \dot{n}_{in}^{j} - \dot{n}_{out}^{j} + \int_{V_r} r^{j} dV$$

3-3

If the reactor is assumed to operate in steady-state, then the conservation laws form a coupled set of equations that can be solved for the boundary conditions shown in Figure 3-1. The AURORA user front for CHEMKIN is commonly used to solve PSR problems for the steady-state reactor temperature and was used to solve all modeling cases presented in this chapter.

3.1.2 Justification for PSR

The recirculation zone downstream of a backward-facing step is characterized by high mixing levels. Vogel and Eaton [6] measured little temperature gradient outside of the near-wall region within the recirculation zone of un-cooled steps— strong evidence of a well-mixed recirculation zone behind un-cooled steps. With film-cooling present, the momentum blowing ratio of the cooling jet must be

"sufficiently small" to not alter the structure of the recirculation zone flow. Since Lewis and Schmidt numbers are typically near unity, it is plausible that the spatial chemical composition of the structurally unaltered recirculation zone is also homogeneous. A PSR model, therefore, is an appropriate choice to model the combustion behind film-cooled backward facing steps with structurally unaltered recirculation zones.

3.1.3 Application of PSR

Correctly applying the PSR model to reacting film-cooled backward-facing steps requires careful definition of model boundary conditions. Figure 3-2 shows how the general backward-facing step flow condition can be conceptually modeled as a series of two ideal processes:

1. Adiabatic mixing of coolant flow and recirculated fow.
2. Reaction of mixed flow as described by PSR model.

It is important to note a fundamental assumption of the mixer-PSR model: the mixing time scale is taken as much smaller than the mean particle residence time, i.e. the reactor is always "well-mixed".
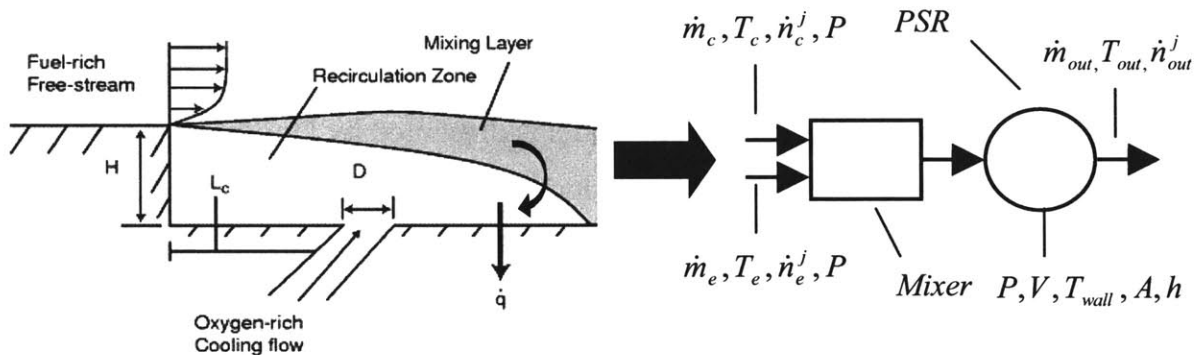

Figure 3-2: Modeling Step as Mixer/PSR

3.1.3.1 Adiabatic Mixing

Mixing between the cooling flow and the flow entrained from the mixing layer precedes chemical reactions. The mixing process is modeled as an adiabatic,

steady-state, non-reacting process. Equations 3-4 & 3-5 are the governing equations for such a process—the conservation of mass and energy, respectively.

$$0 = \dot{m}_c + \dot{m}_e - \dot{m}_{mix} \qquad\qquad 3\text{-}4$$

$$0 = \dot{m}_c h_{t,c} + \dot{m}_e h_{t,e} - \dot{m}_{mix} h_{t,mix} \qquad\qquad 3\text{-}5$$

In equations 3-4 & 3-5, the inlet fluxes into the mixer have been divided between the coolant flow stream and the flow entrained into the recirculation zone from the mixing layer.

Expressions for the inlet fluxes can be determined from physical constraints specific to backward-facing step flow or left as free parameters. Because the model predictions are to be compared with the reacting step experiments detailed in chapter four, physical constraints consistent with backward-facing step flow are imposed to find the inlet fluxes.

Total mass flow into the theoretical mixer is the sum of cooling flow and the flow entrained from the mixing layer. If freestream flow conditions are known and a mass blowing ratio is assumed, then the coolant mass flow is known for a given cooling hole geometry. Because a known cooling gas is used with a given temperature, the total coolant gas enthalpy is also known.

Specifying the magnitude of the entrained fluxes requires a bulk transport model across the mixing layer. This model is presented by Underwood [11], and adapted for present use as summarized below. The bulk transport of mass across the mixing layer is defined in terms of an effective normal velocity at the mixing layer/recirculation zone interface

$$\dot{m}_e = \bar{\rho}_o u_n A_o, \qquad\qquad 3\text{-}6$$

where A_o is the area of the mixing layer/recirculation zone interface, and $\bar{\rho}_0$ is defined as

$$\bar{\rho}_0 = \tfrac{1}{2}(\rho_1 + \rho_2). \qquad\qquad 3\text{-}7$$

The interface area, A_o, is found by assuming that the recirculation zone has a triangular cross-sectional area, with leg lengths equal to the step height and reattachment distance. The effective normal velocity is given by

$$u_n = C_{dif} v_D ,$$ 3-8

where v_D is the average normal shear layer velocity. If laminar mixing effects are neglected, then the average normal shear layer velocity is given by

$$v_D = C_1 u_{dif} ,$$ 3-9

where u_{dif} is defined as

$$u_{dif} = u_1 - u_2 .$$ 3-10

The coefficient, C_{dif}, in equation 3-8 is parameterized as a multiple of the mixing given by the planar shear layer studied by Hermanson and Dimotakis [12] (*e.g.* $C_{dif} = 5$ corresponds to 5 times the mixing in a planar shear layer). The constant, C_1, in equation 3-9 is found by assuming an error function profile for the velocity across the shear layer and using the 5% and 95% velocity points to compute C_1, yielding a value of $C_1 = 0.092$.

To fully define the inlet flow into the adiabatic mixer, the specific enthalpy of the entrained flow must be specified. The mole fractions and temperature of the entrained flow are assumed to be the same as the freestream flow, and thus the specific enthalpy term can be determined.

3.1.3.2 Perfectly Stirred Reaction

After mixing, combustion can be modeled with the perfectly-stirred reactor. The perfectly stirred reactor model is presented in section 3.1.1, and the present section demonstrates how each input term is determined. For a perfectly-stirred reactor operating in steady-state, the mass, energy, and molar conservation equations are

$$0 = \dot{m}_{in} - \dot{m}_{out} ,$$ 3-11

$$0 = h_{conv} A_{wall} (T_{wall} - T_{t,reac}) + \dot{m}_{in} c_{P,in} T_{t,in} - \dot{m}_{out} h_{t,out} ,$$ 3-12

$$0 = \dot{n}_{in}^j - \dot{n}_{out}^j + r^j V .$$ 3-13

The input parameters typically required for closure of the perfectly-stirred reactor model are listed in Table 3-1.

43

Table 3-1: PSR model input parameters

$\dot{m}_{in}$	Inlet massflow
h_{conv}	Average surface convective coefficient
A_{wall}	Wall boundary surface area
T_{wall}	Wall boundary temperature
$T_{t,in}$	Inlet total temperature
$\dot{n}_{in}^{j}$	Inlet molar flow rate for species j
V	Reactor volume
P	Reactor pressure

The physics of film-cooled backward-facing step flow is carefully considered when assigning values to each input parameter. The inlet massflow, total temperature, and molar flow rate are determined by applying the adiabatic mixing model described in section 3.1.3.1. Turbulent flow over a backward-facing step typically reattaches 6-8 step heights downstream of the step face. As seen in Figure 3-2, the cross-sectional area of the recirculation zone can be approximated as triangular, and thus the wall boundary surface area and reactor volume can be estimated. The average surface convective heat transfer coefficient is found by performing an area average on the convective coefficient profile measured downstream of a backward-facing step by Seban, et al. [5],

$$h_{conv} = \frac{1}{L_{wall}} \int h(L)dL.$$ 3-14

The last two parameters, reactor pressure and wall boundary temperature, are left as free parameters and assumed given for each case.

3.2 Parametric Study

This section presents the results of applying the adiabatic mixer/PSR model to several backward-facing step flow scenarios. Results are presented in terms of the reduced set of dimensionless parameters, described in section 2.4.1, to facilitate comparison with experimental data.

3.2.1 Simulated Conditions

Table 3-2 lists the range of parameters spanned in the modeling study. The values of freestream pressure, wall temperature, and coolant temperature were chosen to match experimental conditions described in chapter four.

The chemical composition of the freestream and cooling flows in the parametric study were chosen to match the gases used in the reacting experiments. As described in chapter four, the freestream was argon seeded with ethylene, and the coolant flow was compressed air supplied at room temperature.

Careful consideration of backward-facing step flow physics motivated the choice of unity for the diffusion coefficient, C_{dif}. The Chapman model [13] for backward-facing step flow postulates that mass exchange between the mixing layer and the recirculation zone is a balance between shear layer entrainment into the mixing layer and pressure driven backflow into the recirculation zone near the reattachment point. Eaton and Johnston [14] found that the border, downstream of the step face, between the mixing layer and the recirculation zone closely matches the structure of a plane shear layer until roughly half of the reattachment distance.

Given the experimental results of Eaton and Johnston [14] and the postulate of Chapman [13], the mass transport can be conceptually divided into two regions: plane shear layer entrainment from the recirculation region into the mixing layer, extending from the step face to half the downstream reattachment distance; and pressure driven backflow from the mixing layer into the recirculation region, extending from half the downstream reattachment distance to the reattachment point. Neglecting curvature of the recirculation zone border, both mass transports occur across the same area. In steady-state, this means that the shear layer entrainment mass flux must balance the backflow mass flux. When no blowing is present, density changes are negligible when the Mach number is sufficiently low, and the characteristic velocity of the pressure driven

backflow must equal the characteristic velocity of the shear layer entrainment. With film cooling present, Cdif is approximately unity if changes in recirculation zone flow structure can be neglected.

Table 3-2: Range of parameters spanned in modeling

$Da = \dfrac{\tau_{flow}}{\tau_{chem}}$	0.15-21
$H^* = \dfrac{\Delta H}{H_\infty}$	0.10-0.40
$B = \dfrac{\rho_c u_c}{\rho_\infty u_\infty}$	0.125-2.0
Step Height	2-10 mm
Freestream Pressure, P	6 atm
Cdif	1
T_{wall}	380 K
T_{cool}	300 K

The parameters presented in Table 3-2 were used in a parametric study of the adiabatic mixer/PSR model presented in section 3.1. Sections 3.2.2 and 3.2.3 show graphical trends of how scaled heat flux changes with various independent parameters. As detailed in chapter two, the scaled heat flux is a dependent parameter that depends on the mass blowing ratio, heat release potential, Damköhler number, and geometry.

3.2.2 Q_s variation with Da

Figure 3-3 and Figure 3-4 show how scaled heat flux varies with Damköhler number for a representative backward-facing step flow case with a step height of 10 mm.

Figure 3-3: Q_s variation with Da for $B = 0.5$

Figure 3-3 shows scaled heat flux variation with Damköhler number and mass blowing ratio for a fixed value of mass blowing ratio of 0.5. These data clearly show that scaled heat flux increases as Damköhler number increases. The Damköhler number was altered by changing the freestream temperature. As Damköhler number increases, the characteristic chemical time scale is reduced due to increasing freestream temperature. Chemical reactions, therefore, are more likely to proceed further toward completion, resulting in more chemical energy released and higher scaled heat flux.

The effects of changing heat release potential are also shown in Figure 3-3. Increasing heat release potential has two effects: the smallest Damköhler number at which heat flux augmentation is predicted reduces, and the scaled heat flux for a given Damköhler number increases. Increasing heat release potential for a fixed Damköhler number reduced the argon present in the freestream. Argon acts as a diluent that mitigates PSR combustion, and more complete reactions, therefore, are promoted as heat release potential increases.

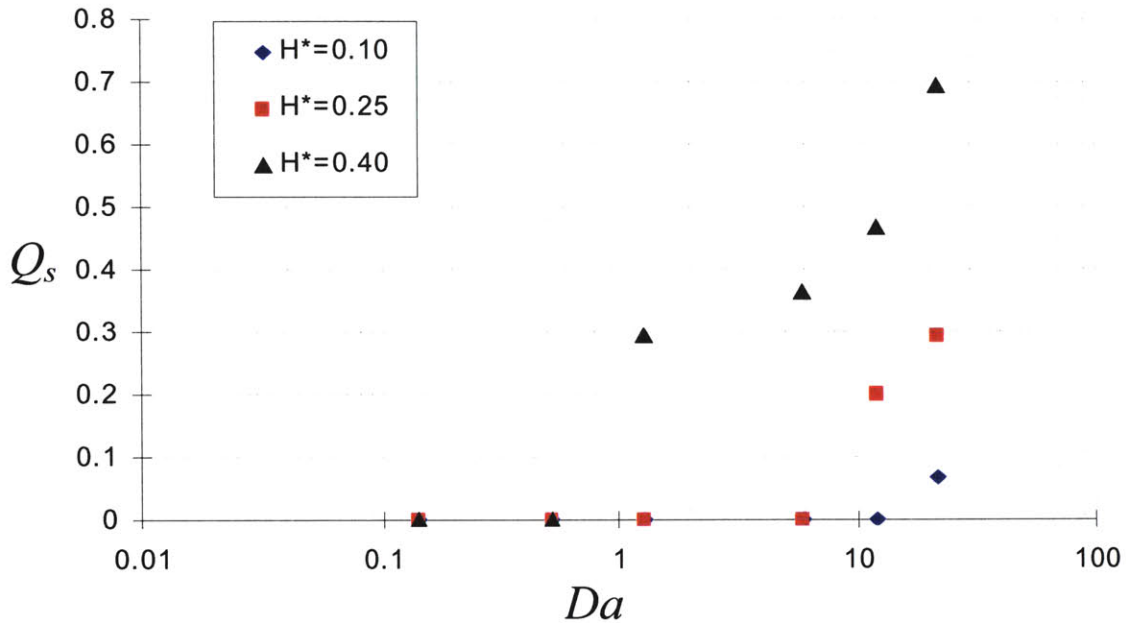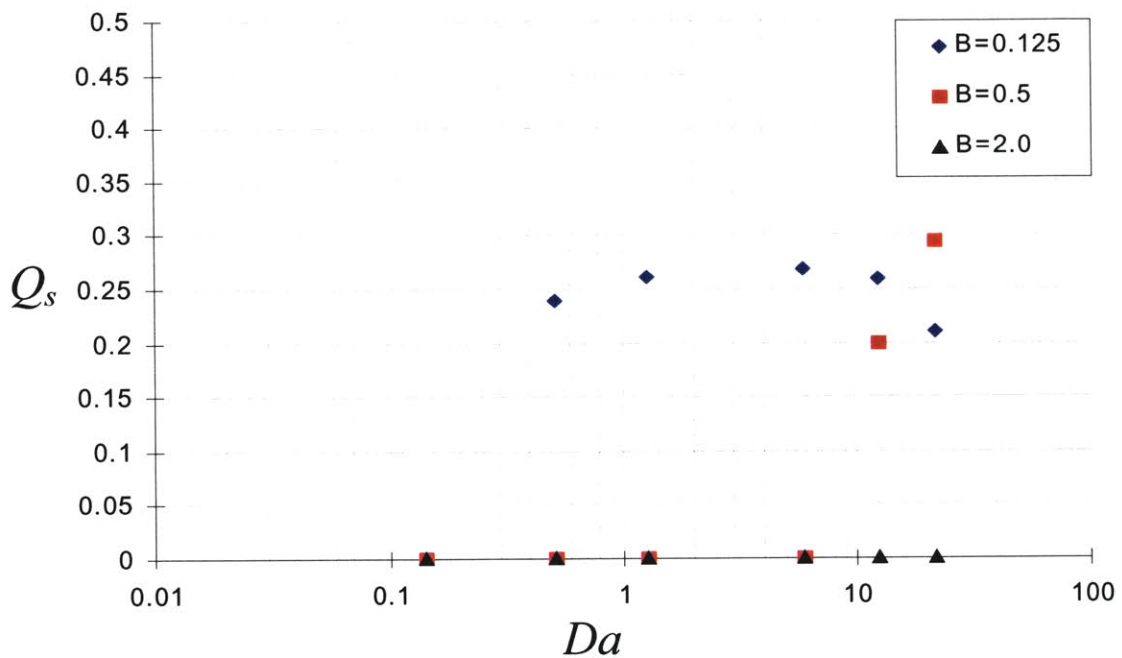**Figure 3-4: Qs variation with Da for $H^*=0.25$**

Figure 3-4 shows scaled heat flux variation with Damköhler number for a fixed value of heat release potential of 0.25. No scaled heat flux was predicted for the highest value of mass blowing ratio modeled, $B = 2.0$. At this mass blowing ratio, the reactor was too lean to support reactions—even at the highest Damköhler number—because of the increased coolant flow. When the mass blowing ratio was reduced to 0.125, combustion occurred over an increased range of Damköhler numbers. For this mass blowing ratio value, the reactor was near stoichiometric fuel-to-air ratio for most of the Damköhler numbers tested. As Damköhler number increases, the amount of fuel required to maintain a

constant value of heat release potential increases due to increasing freestream temperature. For the $B = 0.125$ case shown in Figure 3-4, the increased fuel level leads to a fuel rich reactor and begins to reduce the scaled heat flux past Damköhler number of approximately 10.
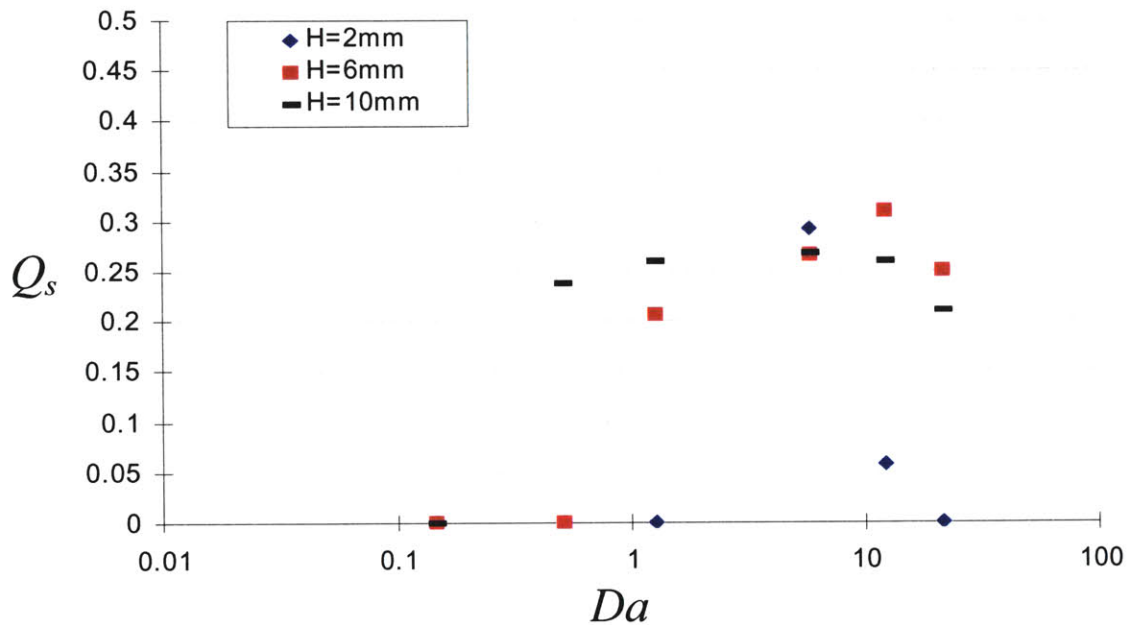

Figure 3-5: Q_s **variation with** *Da* **for various step heights**

Figure 3-5 shows the scaled heat flux variation for three different step heights: 2 mm, 6 mm, and 10 mm. The mass blowing ratio and heat release potential were fixed at 0.125 and 0.25, respectively, for this trend study. The complex trends of scaled heat flux variation with step height are clearly shown in Figure 3-5. Higher scaled heat flux is not necessarily associated with the larger step height. As the step height increases, however, the range of Damköhler numbers over which scaled heat flux is predicted increases. The clear message from Figure 3-5 is this: as step height increases the range of Damköhler number that sustains combustion increases, but given the right conditions, even a small step height can sustain combustion. This is because as step height increases, the sensitivity of recirculation zone equivalence ratio to Damköhler number

decreases, which leads to a broader range of Damköhler numbers over which the recirculation zone has fuel and oxidizer in combustible proportions.

3.2.3 Step height effects on Qs

One of the research goals posed in section 1.3 was to be able to determine the minimum step height needed to support reactions for any given thermodynamic or fluid dynamic conditions. Stated in terms of the governing non-dimensional parameters: what is the minimum step height for which Q_s is positive for any given H^*, Da, and B?

The adiabatic mixer-PSR model was used to predict scaled heat flux values for a range of step heights. Step heights from 2 mm to 10 mm were tested for a variety of H^*, Da, and B values.

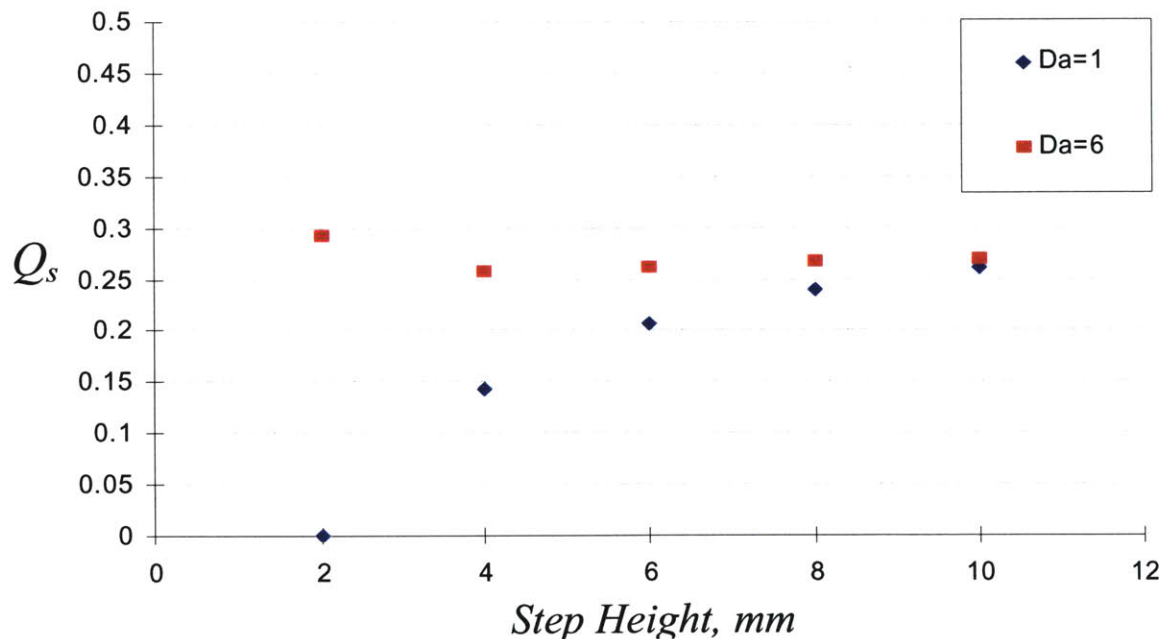**Figure 3-6: Step Height effects on Q_S, with $B = 0.125$ and $H^* = 0.25$**

Figure 3-6 shows the effects of step height on scaled heat flux. All of the cases shown in Figure 3-6 have mass blowing ratio and heat release potential values equal to 0.125 and 0.25, respectively. As the step height is decreased there are two competing effects on the scaled heat flux. Reducing the step height

50

reduces the characteristic flow time, and the characteristic chemical time must reduced to maintain a constant Damköhler number. The freestream temperature, therefore, increases as the step height decreases. Because the heat release potential is constant, the argon diluent in the freestream decreases as the step height decreases. Less argon is present to mitigate reactions as the step height decreases, and more complete combustion is promoted. Decreasing step height also reduces the area through which mass is exchanged between the mixing layer and the recirculation zone. Less fuel is entrained, and the recirculation zone becomes leaner. If the recirculation zone already has more oxidizer than stoichiometric reaction requires, then less entrained fuel mitigates scaled heat flux.

In Figure 3-6, the lower Damköhler number case is dominated by the reduction of entrained fuel effect. As the step height decreases, the scaled heat flux is gradually reduced until no combustion is sustained at the lowest step height tested. The higher Damköhler number case is initially dominated by the reduction of entrained fuel, as seen by the reduction of the scaled heat flux when the step height is reduced from 10 mm to 4 mm. Further reduction in step height, however, switches the dominant effect to the reduction in argon diluent, as seen by the increase in scaled heat flux when the step height is reduced from 4 mm to 2 mm. That the argon diluent effect occurs in the higher Damköhler number case is plausible. As Damköhler number increases, the freestream temperature increases. If the same heat release potential is maintained, then higher adiabatic flame temperatures are required for the higher Damköhler number cases. Less argon diluent is, therefore, present in the higher Damköhler number cases. The reduction in argon diluent due to increased Damköhler number couples with the argon reduction due to decreasing step height previously described, and potentially dictates the trend of scaled heat flux, as seen in Figure 3-6.

51

The effects of mass blowing ratio on scaled heat flux for various step heights are shown in Figure 3-7. Damköhler number and heat release potential were held constant at 6 and 0.25, respectively. As mass blowing ratio increases, less scaled heat flux is predicted because the recirculation zone is leaner and has a reduced inlet temperature due to an increased coolant flow injection. As the step height decreases, the decrease in entrained fuel makes the recirculation region even leaner, and the scaled heat flux is mitigated.
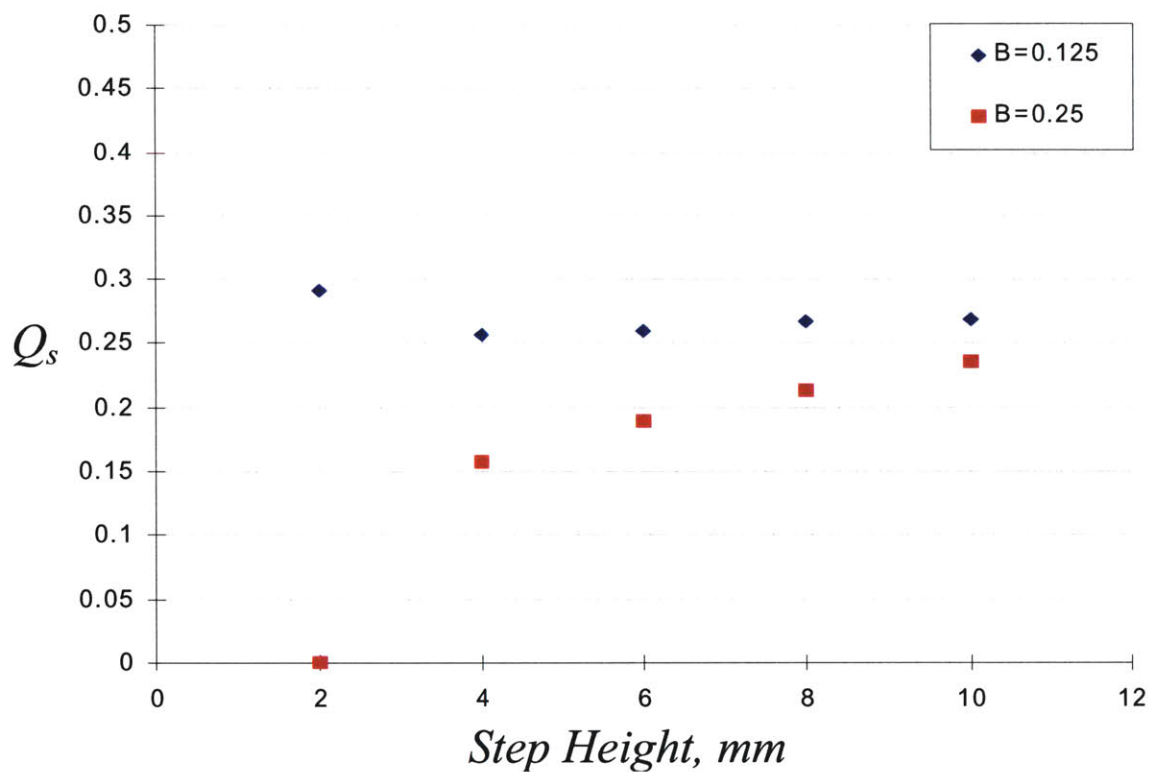
Figure 3-7: Step height effects on Q_s with fixed $Da = 6$ and $H^* = 0.25$

Figure 3-8 shows the effect of heat release potential on scaled heat flux for a range of step heights. Damköhler number and mass blowing ratio were held constant at 6 and 0.125, respectively. As the heat release potential is decreased, scaled heat flux is mitigated. The recirculation zone is leaner than the high heat release potential case, and as step height is reduced, the reduction in entrained fuel dominates the scaled heat flux trend.

Q_s

Step Height, mm

H*=0.1
H*=0.25

Figure 3-8: Step height effects on Q_s with fixed $Da = 6$ and $B = 0.125$

3.3 Chapter Summary

A reduced order mixing/PSR model was developed to predict scaled heat flux in the recirculation region of film-cooled backward-facing steps. A range of the reduced set of dimensionless parameter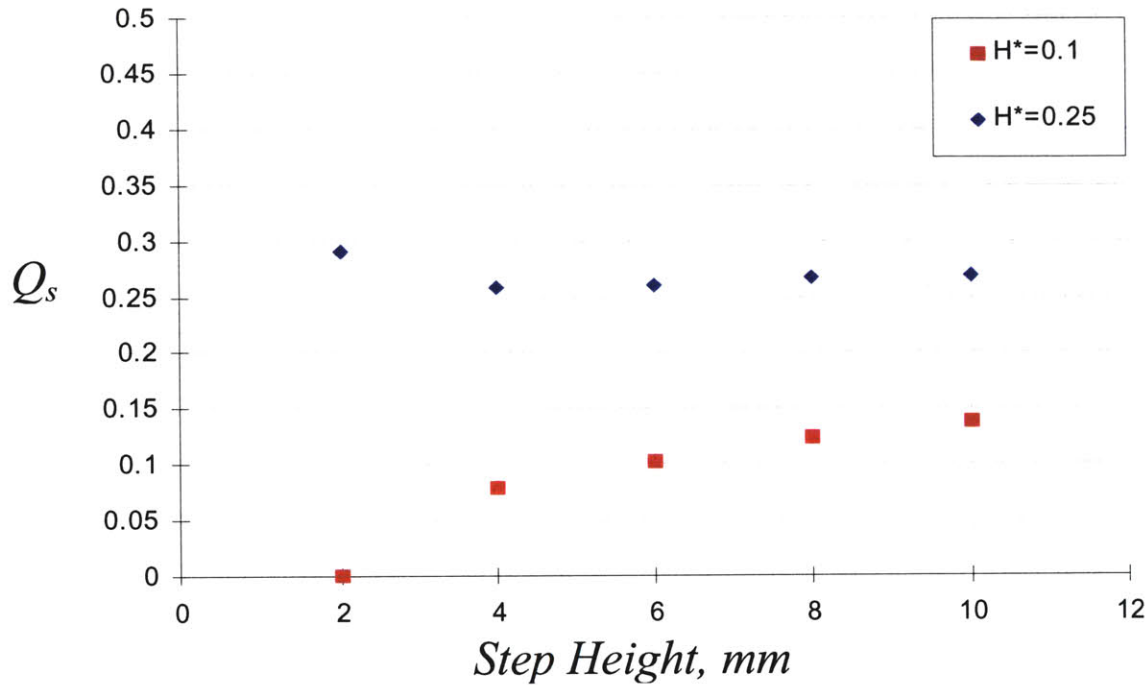s, described in section 2.4.1, were tested for a parametric study of the model. The study showed that mass blowing ratio, Damköhler number, and heat release potential all affect the scaled heat flux value.

As the mass blowing ratio is increased with the Damköhler number held constant, the local equivalence ratio in the recirculation zone lessens. If the recirculation zone was fuel rich before the increase in mass blowing ratio, then the local equivalence ratio shifts closer to unity, which promotes higher scaled heat flux values, as shown in Figure 3-4 for the highest Damköhler number case. If the increase in coolant flow causes the recirculation zone to be more fuel lean, then scaled heat flux values are lowered.

Increasing the heat release potential for a fixed Damköhler number results in more fuel being present in the freestream. More fuel, therefore, becomes entrained into the recirculation zone. If the recirculation zone is fuel lean before the increase in heat release potential, then increasing H^* promotes higher scaled heat flux. If the recirculation zone is fuel rich before the increase in heat release potential, then there are two competing effects that determine how the scaled heat flux changes. Increasing the fuel entrained into the recirculation zone further increases the local equivalence ratio past unity, which mitigates combustion, but increasing H^* also reduces the proportion of combustion mitigating argon present (assuming the freestream mass flow remains fixed), which promotes combustion. Therefore, scaled heat flux can increase or decrease depending on which effect dominates.

This balance of competing trends described in the previous paragraph also applies to what effects changing Damköhler number and step height have on scaled heat flux, as seen in Figure 3-4 and Figure 3-6. Increasing the Damköhler number promotes combustion by raising the freestream temperature and reducing the proportion of argon in the freestream. The amount of fuel present in the freestream increases, which can mitigate reactions if the recirculation zone is already fuel rich. Decreasing the step height while fixing the Damköhler number lessens the entrainment of the freestream flow into the recirculation zone. With less freestream entrainment, less fuel and argon are present in the recirculation zone. If the recirculation zone were fuel rich before the reduction in step height, then higher values of scaled heat flux are promoted with reduced entrainment. If the recirculation zone were fuel lean before the reduction in step height, then the scaled heat flux can either increase or decrease depending on whether the effect of changing fuel level or argon level dominates.

As the dependent non-dimensional parameters are altered, there are often competing effects that dictate the trend of the scaled heat flux: more entrained flow from the mixing layer increases the fuel in the recirculation zone, but also

increases the presence of combustion mitigating argon; and vice versa for less entrained flow. Combustion in the recirculation region behind film-cooled backward-facing steps is a difficult problem, and several of the competing effects, which are not intuitively obvious, were shown in the parametric study and are summarized in the following paragraphs.

Chapter 4

4 Reacting Step Experiments

This chapter describes reacting film-cooled backward-facing step heat flux experiments performed in the MIT Gas Turbine Laboratory shock tunnel facility. The first section introduces the test facility and instrumentation. A test matrix is developed in the second section to elucidate how the scaled heat flux ratio is affected by varying mass blowing ratio, heat release potential, and Damköhler number. Figures illustrating experimentally measured trends are then presented, in both dimensional and non-dimensional space, and analyzed.

4.1 Test Facility and Instrumentation Overview

The shock tunnel facility is a short duration high temperature research facility located within the MIT Gas Turbine Laboratory. For several reasons, it is well suited for housing reacting film-cooled backward-facing step heat transfer experiments. Its potential to provide a high pressure and high temperature testing environment makes it attractive for heat transfer studies with the potential to span a wide range of non-dimensional operating space. Due to its test chamber design, test pieces with a wide range of sizes and shapes can be studied—including test pieces that have surface film cooling. Kirk's [2] demonstration of accurate, high frequency response surface temperature measurements validate the use of this facility for short duration heat flux measurements.

4.1.1 Shock Tunnel Facility Description

The shock tube consists of a 7.3 m driven section and an 8.4 m driver section. Both sections are made of 30 cm diameter steel pipe. The shock tube and diaphragm sections are suspended on linear rollers to allow access to the

diaphragm sections during test preparation. Figure 4-1 shows a schematic of the MIT shock tunnel facility with its linear roller track.
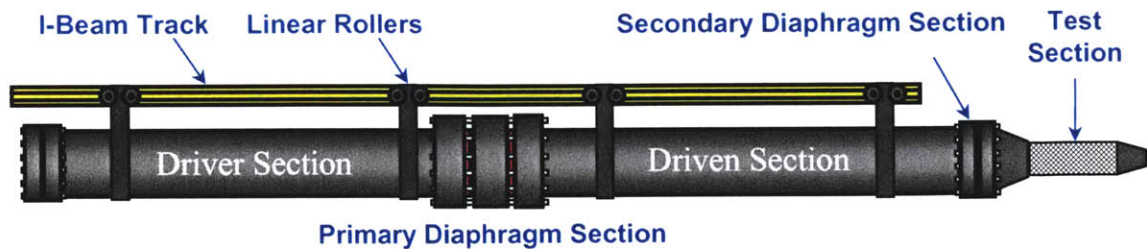

Figure 4-1: Shock tunnel on linear rollers

Before each test, aluminum diaphragms are placed on each side of the primary diaphragm section to enable each tube section to fill to a different pressure. A thin metal diaphragm is placed at the end of the test section so the driven section can be evacuated. The driver and primary diaphragm sections are filled with a combination of helium and argon to a pressure of 4-6 atm, and the driven section is evacuated and then filled with a combination of argon and ethylene to a pressure of 0.1 atm. Test articles are placed within the test section. A test is initiated by rapidly evacuating the primary diaphragm section; the impulsive pressure difference is sufficient to rupture the metal diaphragms. The instantaneous discontinuity in pressure causes a shock wave to propagate through the driven section, as described by Kirk [2]. After the shock wave propagates through the test section, a high temperature and high pressure freestream flow passes over the test article and out of the test section. The shock tunnel facility was designed to provide freestream test conditions of 6 atm pressure and 1200-2800 K temperature. For a detailed design and analysis of the shock tunnel facility, the reader is referred to Kerwin [15].

4.1.2 Test Articles

Test articles were designed to withstand the high temperature and pressure freestream conditions inside the test section of the shock tunnel, replicate film cooling flow conditions, and allow high frequency heat flux measurements. Due

to the short test times, on the order of 20 ms, MACOR test pieces were used, which aided in the surface heat flux measurements.

4.1.2.1 Film-Cooled Flat Plate

Figure 4-2 shows the test plate used during the reacting film-cooling experiments. The plate is 3"x10" with a leading edge angle of 25°. The leading edge of the test plate was made of aluminum to withstand the high heat load present at the freestream flow stagnation point. The surface of the flat plate was covered with a 0.1" thick sheet of MACOR; the low thermal conductivity of MACOR facilitated surface heat flux measurements. A spanwise row of eight 0.1" diameter cooling jets are located at a distance of 2.2" from the plate leading edge. The center-to-center cooling hole spacing is 0.3". The cooling jets, inclined at an angle of 35°, are grouped into two sets of four, with the plate's line of symmetry dividing the two groups. Different gases can be blown into each group allowing for simultaneous testing of reacting and inert cooling gases. High frequency temperature gauges located behind the cooling holes enable rapid sampling of the plate surface temperature.
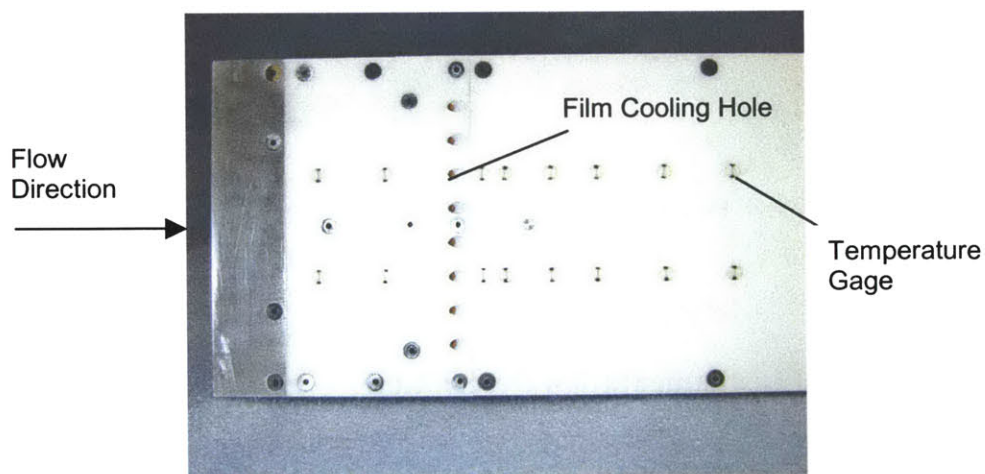

Figure 4-2: Film-cooled test plate

4.1.2.2 Film-Cooled Backward-facing Step

The existing film-cooled flat plate was modified by attaching a step piece to the leading edge as shown in Figure 4-3. This simple solution enabled backward-facing step tests to be run with minimal alteration of previously proven equipment. The step height is 0.4″, and the distance from the step face to the center of the cooling holes is 0.2″. These values corresponded to $L_c^* = 2$ and $D^* = 4$.
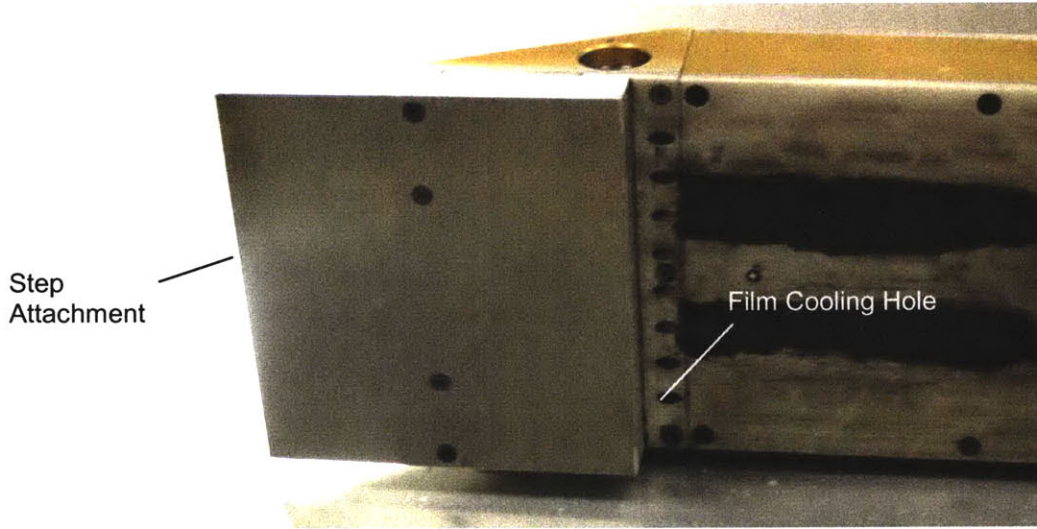

Figure 4-3: Test plate with step attachment

4.1.3 Experimental Instrumentation Description

Capturing temperature measurements during the short duration shock tunnel tests required the use of high frequency response instrumentation. Platinum RTD gauges were used in conjunction with an ADTEK MMADCAP data acquisition system to provide plate surface temperature measurements with a

sampling frequency of 100 kHz. The instrumentation is identical to that used by Kirk [2] to measure plate surface temperature history during short duration tests.

4.1.3.1 Temperature Gauges

Figure 4-4 shows a high-frequency temperature gauge. The gauge is made of 1/8" MACOR cylinder with a platinum resistance element painted on the tip of the cylinder. The thickness of the resistance element, painted with a single hair brush, is small enough so that the gauge provides negligible conduction heat transfer resistance. Therefore, the gauge temperature directly indicates the plate surface temperature. Using the ACQ processing method described by Kirk [2] and in more detail by Vidal [16], the temperature versus time profile can be integrated to determine surface heat flux if the material properties of the surface are known.
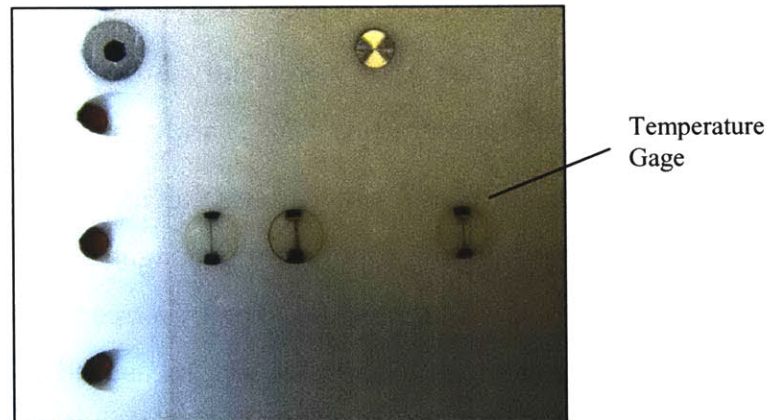

Figure 4-4: Detail view of temperature gage

4.1.3.2 Data Acquisition System

An ADTEK MMADCAP data acquisition system is used to sample the signals from the temperature gauges. The sampling rate was 100 kHz, with a sampling window of 6 seconds. Each surface temperature gage sent a signal to a different

channel on the board so that all gages could be simultaneously monitored and recorded.

4.2 Testing Plan and Procedure

Reacting film-cooling experiments were performed to assess the heat flux augmentation behind backward-facing steps. Tests were run for a range of non-dimensional parameters. Results show that for $Da \sim 10$ and $B = 0.5$, the scaled heat flux augmentation can be as high as 75%, compared to 55% for the same non-dimensional conditions in the flat plate.

4.2.1 Experimental Uncertainty Analysis

All experimental plots are shown with uncertainty bars. The procedure used to calculate the range of experimental uncertainty is presented in detail by Kirk [2] and summarized in this section.

The two largest sources of uncertainty in the reacting step experiments were the freestream temperature, $T_{t,\infty}$, and the convective heat transfer coefficient, h. Uncertainty in h only affects calculation of scaled heat flux, but uncertainty in the freestream temperature propagates through the calculation of many quantities such as Da, St, and Re. The freestream temperature is known to within 10% using ideal shock theory for each measured shock speed, as detailed by Kirk [2]. The convection coefficient is taken from [4] with an uncertainty of 10% due to the presence of a film-cooling jet. As suggested in chapter six, a more accurate model of the convection coefficient would reduce the experimental uncertainty associated with the scaled heat flux values.

Other sources of uncertainty are the location of the reattachment point and the value of measured heat flux. The latter, as Kirk suggests, is known to within 1%. The former is located at the point of highest heat flux, and is known to within half the distance between consecutive gages.

4.2.2 Test Facility Benchmark

Figure 4-5 shows Stanton number variation with Reynolds number measured on the flat plate test article with no reactions or film cooling. The measurements, as expected follow the trend of the theoretical turbulent boundary layer Stanton number-Reynolds number correlation for a flat plate, used by Kirk [2]. Each measurement represents a side-to-side average at a particular downstream gage position of the time mean measurements from the air and nitrogen sides. Only the third gage location, the first behind the cooling holes, showed appreciable deviation from the theoretical correlation. Kirk [2] also noticed this on some of his final tests, and he postulated that one of the two cooling gages immediately behind the cooling holes was beginning to fail. This was later confirmed with a gage calibration procedure, as described by Kirk [2].
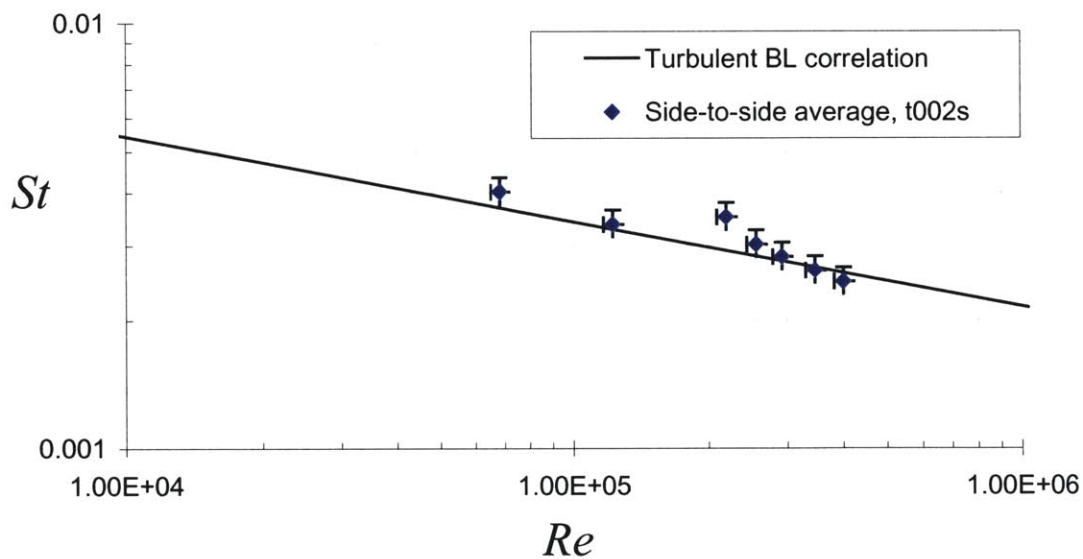
Figure 4-5: Stanton number variation with Reynolds number for flat plate

To validate the performance the shock tunnel facility for backward-facing step tests, non-reacting cases with no film-cooling were compared to published experimental data. Figure 4-6 shows a plot of Stanton number, normalized by the maximum Stanton number value, versus non-dimensional reattachment distance, X^*. The data measured from the shock tunnel runs is compared to the

63

experiment of Vogel and Eaton [6]. As seen in the Figure 4-6, the shock tunnel data matches Vogel and Eaton's measurements closely in both magnitude and trend.

$$X^* = \frac{X - X_r}{X_r}$$
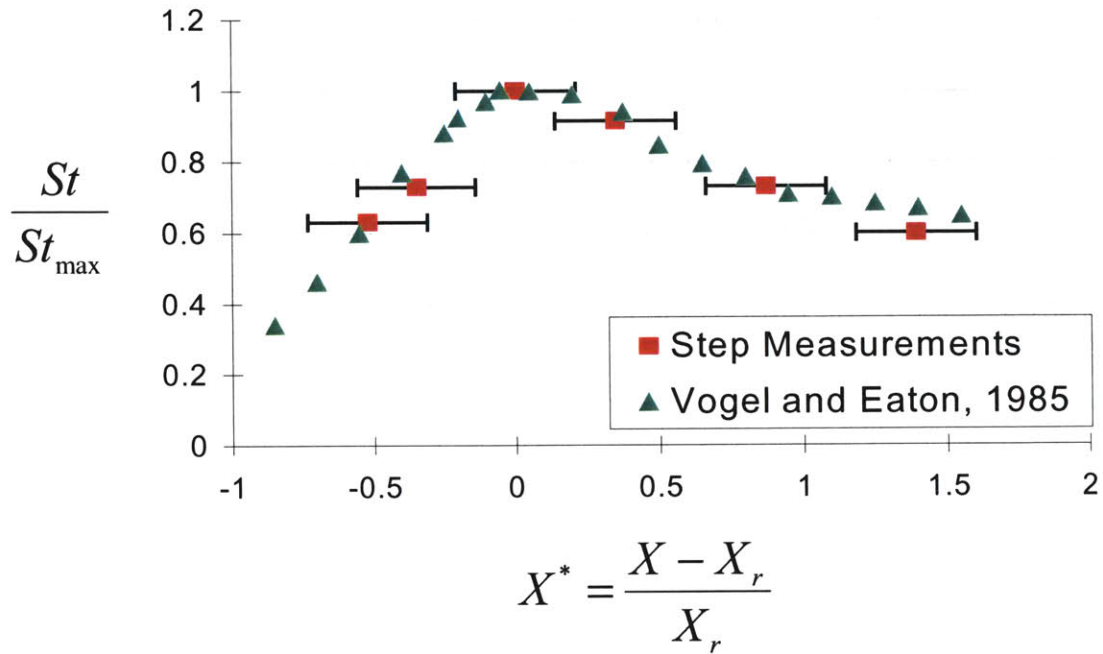
Figure 4-6: Benchmark Stanton number correlation

4.2.3 Test Matrix

The test matrix shown in Table 4-1 was used to span the governing non-dimensional space for the reacting backward-facing step experiments. An set of experimental data was collected in the following way: for a particular mass blowing ratio and heat release potential, different Damköhler numbers were tested starting with the highest and working down. When a Damköhler number was reached where no appreciable heat flux augmentation was measured during the experiment, a new combination of mass blowing ratio and heat release potential was chosen to study and the Damköhler number sweep for that particular combination was performed again. The results of the experiments are presented in the following section.

Values for the parameters in the test matrix were chosen for the following reasons. The mass blowing parameters were selected for direct comparison with the work of Kirk [2]. The values of $B = 0.5$ and 2.0 correspond to an attached and lifted jet, respectively, in the flat plate tests. Damköhler number values were chosen to range from a value much less than unit, approximately 0.05, to the maximum value achievable in the shock tunnel facility, approximately 20. Two intermediate values of unity and ten were selected to assess heat flux augmentation trends at other Damköhler number values. Heat release potential values were chosen to simulate typically CO equivalent energy levels of HFA combustors. Values of $H^* = 0.2\text{-}0.35$ correspond roughly to 30,000-60,000 ppm CO equivalent energy. The value of $D^* = 4$ was chosen because it corresponds to the largest step height that still has an aspect ratio above 8-10—necessary to minimize three-dimensional flow effects near the plate centerline. A value of L_c^* = 2 was selected to keep the cooling hole as close to the step face as possible, thereby maximizing the number of temperature gages in the recirculation zone, while avoiding overlap of the step face onto the cooling hole if a D^* of unity were ever tested.

Table 4-1: Reacting step test matrix

B	0.5, 2.0
Da	0.05, 1, 10, 20
H^*	0.25, 0.35
D^*	4
L_c^*	2

4.3 Testing Results

Reacting shock tunnel experiments provide insight into the details of heat flux behind film-cooled backward-facing steps. After verifying the fidelity of the shock tunnel facility with a repeatability test, reacting experiments were run over

a range of governing non-dimensional parameters for both the flat plate and the backward-facing step. These experiments measured up to 75% scaled heat flux for the film-cooled backward-facing step with $B = 0.5$ and $Da \sim 10$—compared to approximately 55% scaled heat flux for a film-cooled flat plate test under similar non-dimensional conditions.

4.3.1 Flat Plate Data

As further validation of the experimental facility, a heat flux measurement repeatability test was performed with the film-cooled flat plate. Two runs were performed at the same mass blowing ratio, heat release potential, and Damköhler number. Heat flux is plotted against non-dimensional distance downstream from the cooling holes. Figure 4-7 shows the results of this repeatability test; only gages downstream of the cooling holes are shown because the upstream gages are not used during step experiments. One can see from Figure 4-7 that the two measurement sets match closely in both magnitude and trend. The downstream heat flux profile also matches that measured by Kirk [2] for an attached cooling jet case.
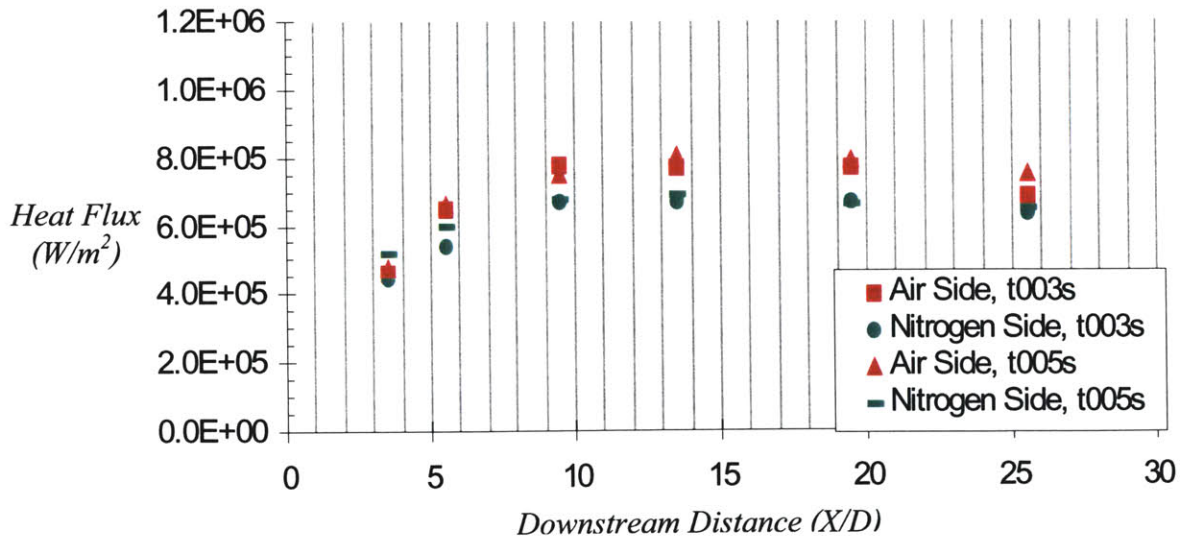

Figure 4-7: Flat plate heat flux measurement repeatability test

4.3.2 Backward-facing Step Data

Figure 4-8 shows the dimensional heat flux measurements for $Da \sim 10$, $B = 0.5$, H^* $= 0.30$ for both the flat plate and $D^* = 4$, $L^* = 2$ step. One can see from this plot that both the reacting and inert side heat fluxes are higher for the step case than the flat plate. This is expected because the recirculation zone and mixing layer interact to produce turbulent eddies that carry large amounts of thermal energy. Many of these eddies are driven back into the recirculation zone by the pressure gradient at the reattachment point, and the heat flux to the wall is augmented. Figure 4-8 shows a 17% increase in heat flux is measured at a downstream location of 10 cooling hole diameters. Because the non-reacting step heat flux is considerably higher than the flat plate heat flux in the same non-dimensional conditions, the 17% heat flux increase due to chemical reactions could pose a greater problem for endwall durability.
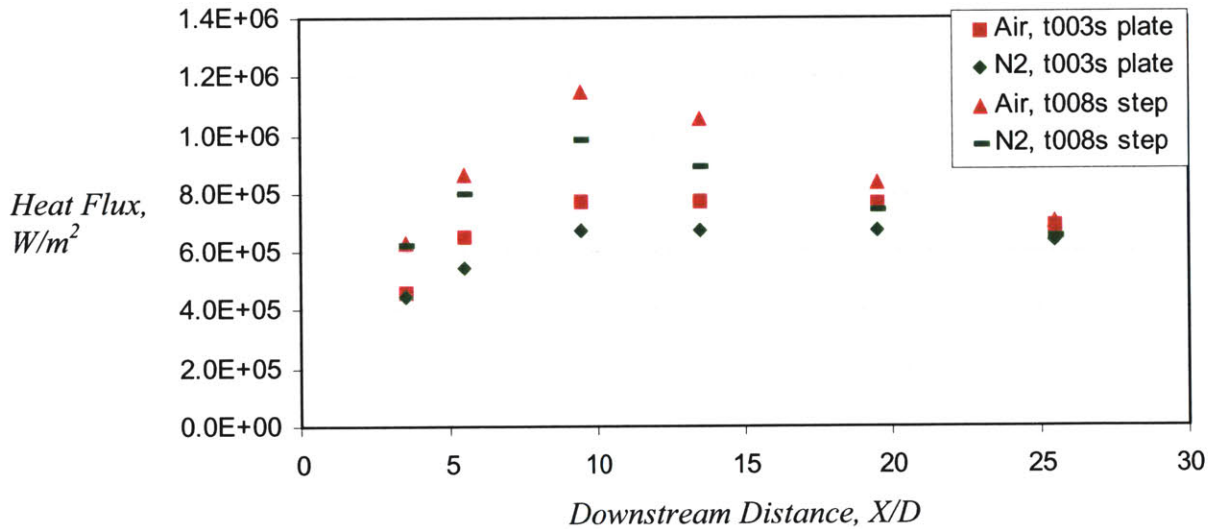

Figure 4-8: Heat flux comparison of step and flat plate

The downstream profile of the maximum scaled heat flux is shown in Figure 4-9 for $B = 0.5$ and $Da = 10$. Different values of heat release potential, ranging from 0.24 to 0.32, are shown in Figure 4-9. The heat flux shown is the maximum value for each gage location measured during the steady-state test

window. Kirk [2] found that scaled heat flux is virtually independent of heat release potential for a reacting film-cooled flat plate. Figure 4-9 shows that this is not the case for reacting film-cooled backward facing steps—only the ends of the uncertainty bars overlap between the highest H^* run and the other two tests. As discussed in detail in chapter three, one would expect scaled heat flux to be a strong function of recirculation zone equivalence ratio, which does depend on the heat release potential. The trends for the different H^* values are similar: quick rise in scaled heat flux followed by a relatively flat region of constant scaled heat flux, and then a decrease in scaled heat flux farther downstream as mixing with freestream mitigates reactions. This trend is similar to the scaled heat flux trend observed by Kirk [2] for a lifted jet on a flat plate.
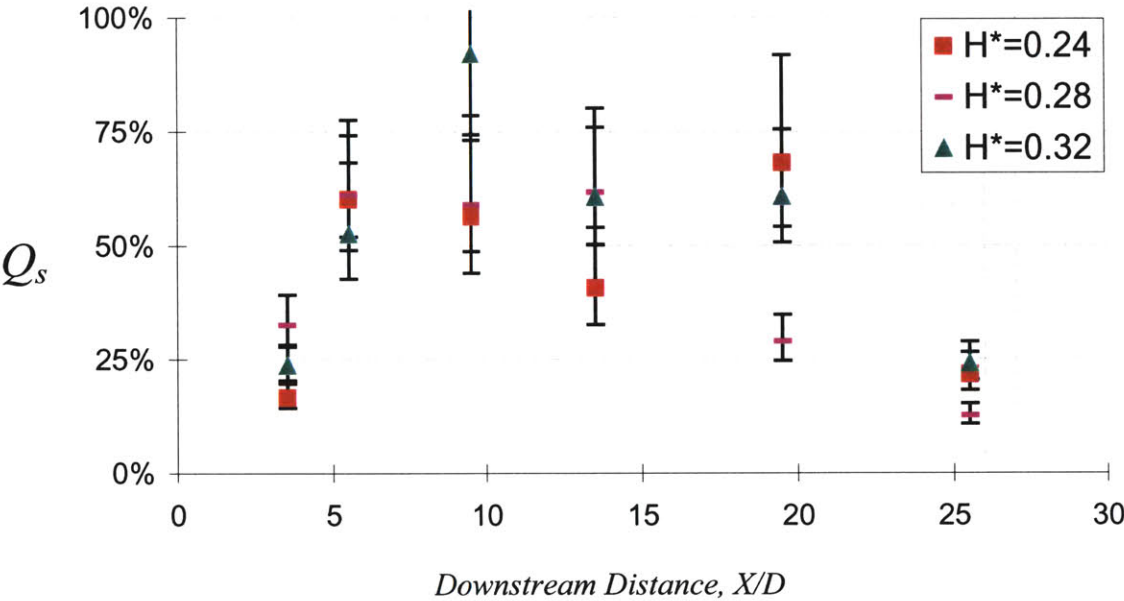

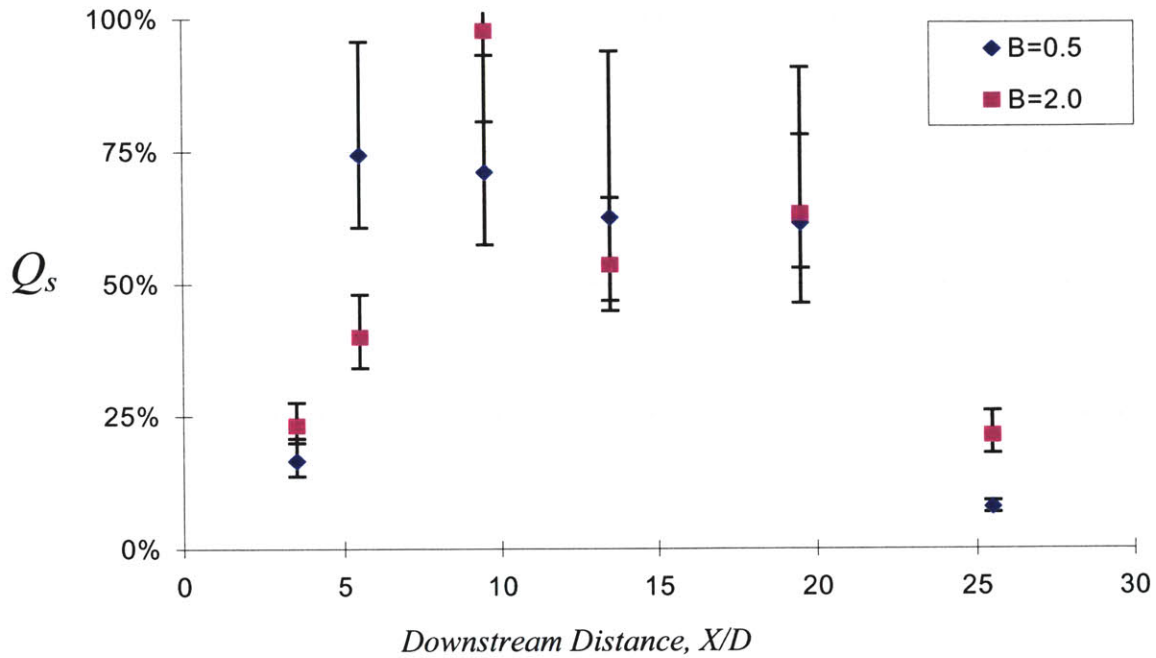Figure 4-9: Q_s downstream profile with various H^*

Figure 4-10: Q_s downstream profile for various B

Figure 4-10 shows the downstream scaled heat flux profile for $Da = 10$ and $H^* = 0.35$ for $B = 0.5$ and 2.0. As in Figure 4-9, the scaled heat flux profile for $B = 0.5$ increases quickly downstream, settles into a relatively constant region, and then decreases. The trend seen for $B = 2.0$ is similar to the $B = 0.5$ trend for the last three gauges, but profile for the first three gages is different. The scaled heat flux appears to increase linearly until a maximum of 95% at $X/D \sim 10$, unlike the $B = 0.5$ case that suddenly jumps to a maximum value and then levels at a constant value for roughly 15 cooling hole diameters downstream.

A comparison between scaled heat flux profiles for the film-cooled step and flat plate are presented in Figure 4-11. Both tests had $Da \sim 10$ and $H^* \sim 0.3$. The two tests show very similar trends: a sharp rise in scaled heat flux followed by a region of constant scaled heat flux. It is plausible to conclude that based on the striking similarity in downstream scaled heat flux profile between the step B

69

= 0.5 case and the plate B = 2.0 case that both have similar flow structure. Thus, the flow structure of the backward-facing step shown in Figure 4-11 is similar to that of a lifted film-cooling jet over a flat plate.
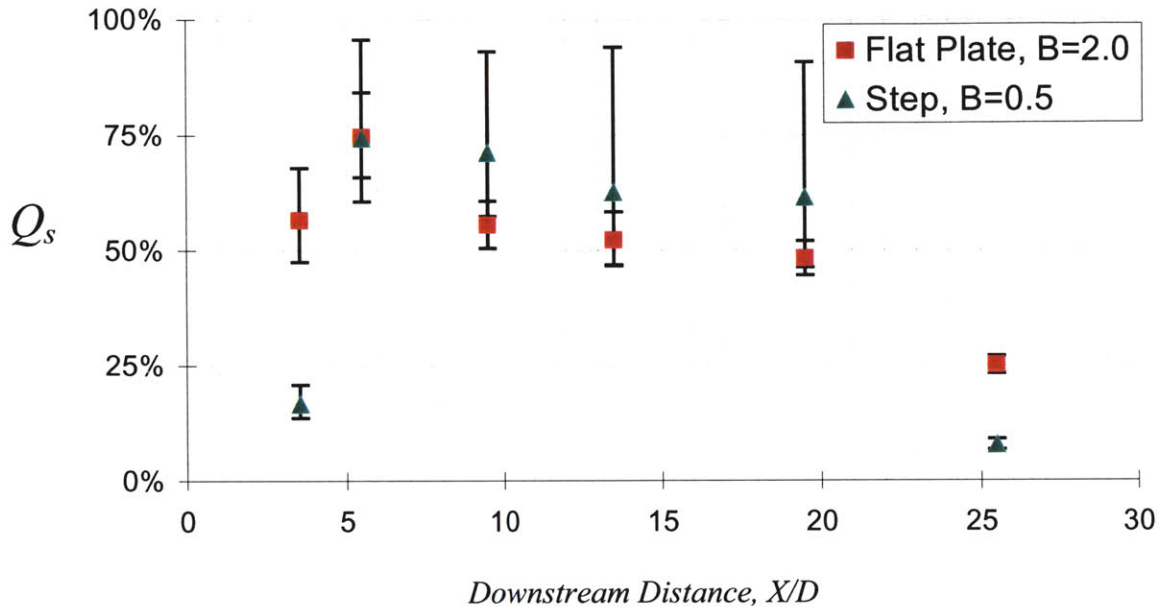
Figure 4-11: Q_s profile similarity between step and flat plate

The presence of the backward-facing step could explain the similarity between scaled heat flux profiles shown in Figure 4-11. Because the recirculation region behind the backward-facing step is characterized by low momentum recirculating fluid, a cooling jet of a given momentum flux has a higher effective momentum blowing ratio behind the step than the same jet would on a flat plate. Cooling jets that would stay attached to the surface of a flat plate could lift from the surface when placed behind a backward-facing step with the same freestream conditions.

Backward-facing steps, therefore, act to change the fluid dynamic boundary conditions upstream of a cooling jet—essentially fixing a region of low momentum fluid immediately upstream of the cooling jet. If this were the only effect of the backward-facing step, then the scaled heat flux would be expected to follow the trends measured by Kirk [2] and have a maximum downstream value

that is independent of the heat release potential. This, however, contradicts the measurements shown in Figure 4-9, which show a noticeable difference in maximum Q_s for different H^* values. Steps must, therefore, also change the upstream thermodynamic boundary conditions in a way that is a function of H^*.
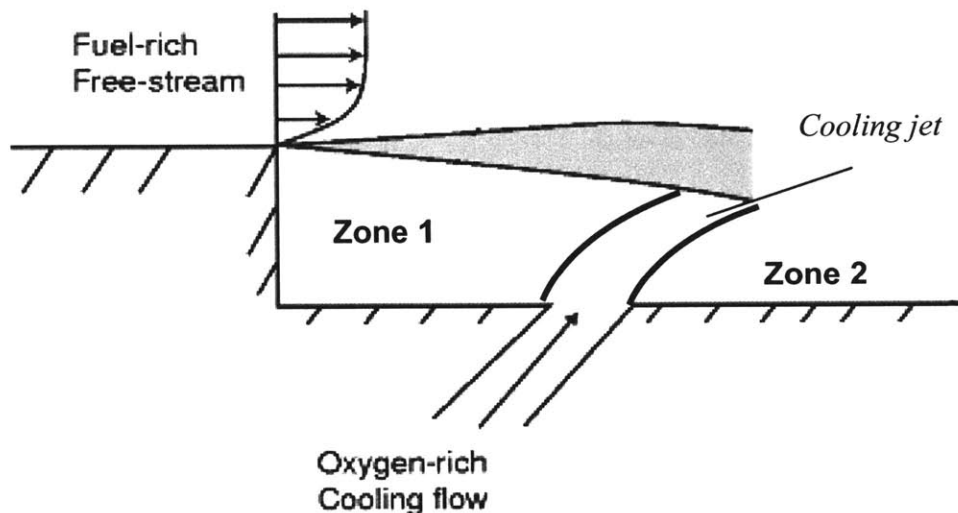
Figure 4-12: Cooling jet splitting recirculation zone

Figure 4-12 shows a schematic of backward-facing step flow with flow zones labeled. The smaller recirculation zone located between the backward-facing step and the cooling jet exchanges mass flow with the mixing layer and the cooling jet. Depending on the freestream and cooling jet fluid dynamic and thermodynamic conditions, the smaller recirculation zone, zone 1, could sustain combustion, so the thermodynamic boundary conditions upstream of the cooling jet can change with heat release potential.

The variation of scaled heat flux with Damköhler number is shown in Figure 4-13. Only negative uncertainty bars are shown for the Damköhler number because the freestream temperature, which is always lower than the value predicted by ideal shock theory, is the dominant factor in Damköhler number uncertainty. Both step and flat plate data are presented for $H^* = 0.24 -$

71

0.87—see appendix A for complete test list. The flat plate data shows the expected trend of H^* independence, and the attached blowing ratio results in higher Q_s.
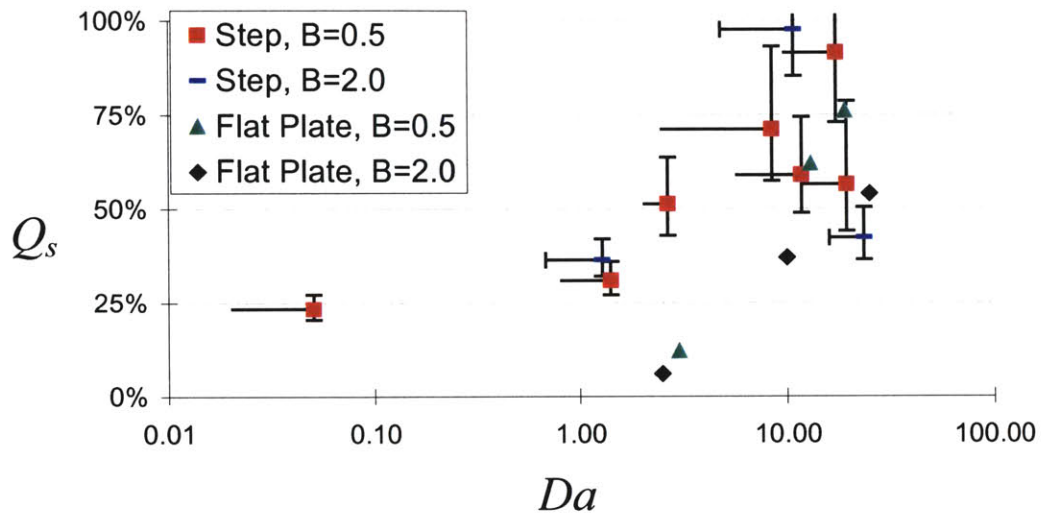

Figure 4-13: Q_s **variation with** Da **for step and flat plate**

The step heat flux data can be divided into two regimes for each blowing ratio, with one regime resulting in significantly higher scaled heat flux for the same Damköhler number. These trends provide further evidence that the small recirculation region located between the step face and the cooling hole alters the upstream thermodynamic boundary of the cooling jet. The higher scaled heat flux measured for the upper regime could result from entrainment of hot gases from this small recirculation region downstream from the cooling hole where the measurements were taken. If the small recirculation region cannot sustain combustion, then it simply alters the upstream fluid dynamic boundary conditions for the cooling jet, as described previously.

Another interesting trend seen in Figure 4-13 is that the upper regime for $B = 2.0$ is characterized by higher scaled heat flux than the upper regime for $B = 0.5$ for the same Damköhler number. Moreover, the lower regime for $B = 2.0$ is characterized by lower scaled heat flux than the lower regime for $B = 0.5$. This could be due to three-dimensional mixing effects. The higher blowing ratio jet

encourages more thorough mixing, so more hot combustion gases from the small recirculation zone are mixed with the fluid downstream of the cooling jet in the upper regime. If combustion does not occur in the small recirculation zone, then the fluid in the recirculation zone is a mixture of freestream and coolant gases. When mixed with the fluid downstream of the cooling jet, these gases mitigate scaled heat flux.

4.4 Chapter Summary

A reacting film-cooled experiment was performed to investigate the heat flux behind backward-facing steps. Results show that the presence of a backward-facing step can significantly increase the heat flux measured downstream of the step face. Measurements presented in the chapter show that scaled heat flux behind a film-cooled backward-step can be significantly higher than the scaled heat flux measured on a film-cooled flat plate under the same non-dimensional conditions. The profile trend of the scaled heat flux variation with non-dimensional downstream distance suggests that there is similarity between backward-facing step flow structure and lifted jet film-cooled flat plate flow structure. The presence of the backward-facing step alters the upstream fluid dynamic boundary conditions for the cooling jet. Unlike the flat plate experimental data, the scaled heat flux measurements for the film-cooled backward-facing step experiments do not collapse for all values of heat release potential. The small recirculation region located between the step face and the cooling jet can also alter the upstream thermodynamic conditions by sustaining combustion.

Chapter 5

5 Comparison of Analytical and Experimental Results

This chapter compares the values of the scaled heat flux predicted by the reduced-order mixer/PSR model to the values measured during the reacting film-cooled backward-facing step experiments. Due to the great discrepancies between predicted and measured scaled heat flux values, it is postulated that the analytical model does not assume the correct recirculation zone flow structure for high blowing ratio cases. A critical value for the momentum blowing ratio, I^*, is proposed to set a bound for the upper limit of I that does not alter the flow structure of the recirculation zone.

5.1 Analytical and Experimental Comparison

This section compares the analytical model predictions with the experimental scaled heat flux measurements. Considerable differences are noted when the cases with mass blowing ratio equal to 2.0 were compared. When the blowing ratio was lowered to 0.5, the trend of scaled heat flux variation with Damköhler number predicted by the model more closely matches the experimental measurements, but there is still a discrepancy in the magnitude of the scaled heat flux values.

5.1.1 Comparison with $B = 2.0$

Figure 5-1 shows evidence that the model does not predict a scaled heat flux profile that matches experimentally measured values. This plot shows the scaled heat flux profile for a mass blowing ratio of 2.0. The model heat release potential parameter was set to 0.25. While the model predicted no scaled heat flux over the range of Damköhler numbers studied—due to excessive oxygen within the recirculation zone, as described in chapter three, the experiments show significant scaled heat flux measurements. Because the model assumed that all

of the cooling flow was injected into the recirculation zone, the fuel-to-air proportions inside the recirculation zone were too lean to support reactions. This discrepancy is likely due to a violation of a fundamental assumption of the mixer/PSR model presented in chapter three; specifically, in the experiments presented in chapter four, the cooling jet with blowing ratio of 2 significantly altered the flow structure of the recirculation zone. Thus, any scaled heat flux predictions obtained from the mixer/PSR model for this blowing ratio were not based on physical assumptions relevant to the actual downstream step flow structure.

The B = 2.0 cooling jets in the experiments could have pierced the recirculation zone, as described in section 4.3.2, and formed a smaller recirculation zone upstream of the jet injection location. Entrainment of the cooling air into this recirculation zone would be some fraction of the total jet mass flow, so the fuel-to-air proportions of this smaller recirculation zone would likely shift to a more fuel-rich value. This would promote reactions in this recirculation zone, and the hot gases produced by combustion could be entrained downstream of the cooling jet by three-dimensional mixing effects around the cooling jet, leading to the high scaled heat flux values measured.
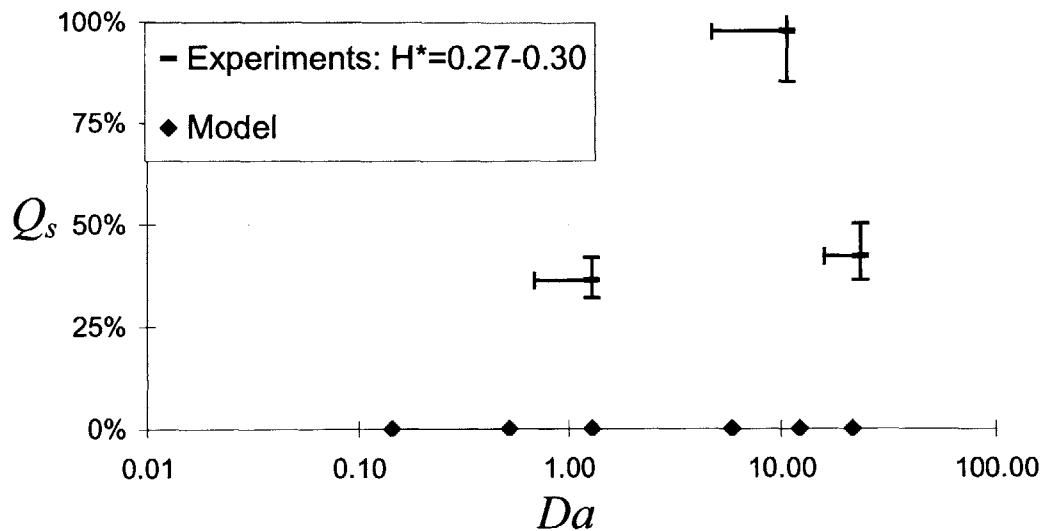

Figure 5-1: Q_s comparison of experiment and model with B = 2.0, H^* = 0.25

5.1.2 Comparison with $B = 0.5$

Figure 5-2 shows the scaled heat flux trend for a mass blowing ratio of 0.5. The heat release potential was fixed at 0.25 for the model predictions. Experiments were run over a wide range of heat release potential values, and the cases with heat release potential closest to the model runs are shown with square bullets. As was the case for $B = 2.0$, there is discrepancy between the model predictions and the experimentally measured values of scaled heat flux. For this mass blowing ratio, however, the model appears to capture some of the scaled heat flux trend measured in the experiments. In the experiments, the scaled heat flux variation with Damköhler number after combustion was sustained was approximately linear for the higher heat release potential values, as seen in Figure 5-2. The model matches this trend, but does not match the magnitude of the scaled heat flux value measured in the experiments. Even though the momentum blowing ratio is low enough for the $B = 0.5$ test runs that the jet likely does not pierce the recirculation zone, see section 5.1.3, the cooling jet could split the recirculation zone into two smaller recirculation zones, as noted by Harinaldi, Ueda, and Mizomoto [7] in non-reacting flow situations. Each recirculation zone would then entrain some fraction of the total cooling jet flow. If the pressure driven backflow remained constant, then the recirculation zone downstream of the cooling jet would be more fuel-rich and, therefore, tend to have higher scaled heat flux values.

A trend measured in the experiments that was not captured by the model predictions was the existence of the lower scaled heat flux regime seen in Figure 5-2 and discussed in chapter four. This could also be a consequence of the double recirculation zones. If the upstream recirculation zone is unable to sustain combustion, then cooler gases could be mixed with the downstream recirculation zone by three-dimensional flows induced by the cooling jet. If the

downstream recirculation zone were still able to sustain reactions, then the extra entrainment of these cool gases would dampen the scaled heat flux, as seen by the lower two squares with $Da > 10$ in Figure 5-2.
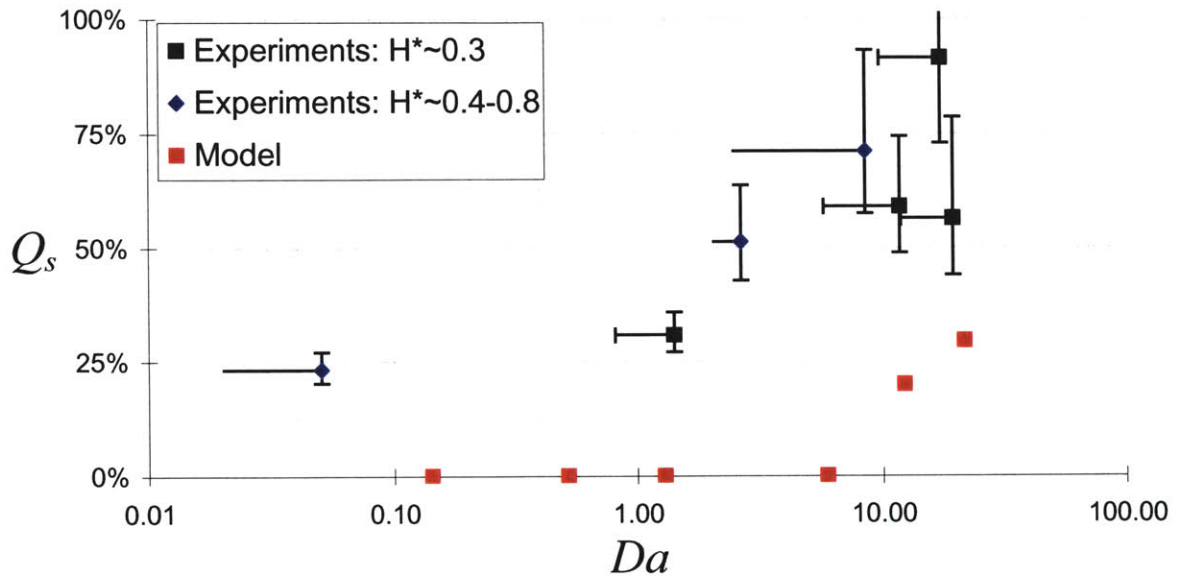
Figure 5-2: Q_s comparison of experiment and model with $B = 0.5$ and $H^* = 0.25$

5.1.3 Critical momentum blowing ratio, I^*

The structure of the recirculation zone is strongly affected by the momentum blowing ratio of the cooling jet, as noted by Harinaldi, Ueda, and Mizomoto [7]. One of the assumptions in the model presented in chapter three was that the recirculation zone flow structure was not affected by cooling jet blowing. For each flow scenario, therefore, an upper bound exists on the momentum blowing ratio, above which, the assumption that the recirculation zone flow structure remains unaltered with blowing is invalid.

A typical cooling jet behind a backward-facing step is shown in Figure 5-3. The cooling jet possesses some component of momentum in the vertical direction due to its inlet angle. If the momentum of the fluid in the recirculation zone is neglected, then the cooling jet impinges upon the mixing layer. Harinaldi, Ueda, and Mizomoto [7] noticed through experimental visualization that the mixing layer is characterized by the presence of coherent eddies whose maximum size and downstream convection speed are functions of the downstream distance from the step face, and the momentum blowing ratio of the cooling jet.
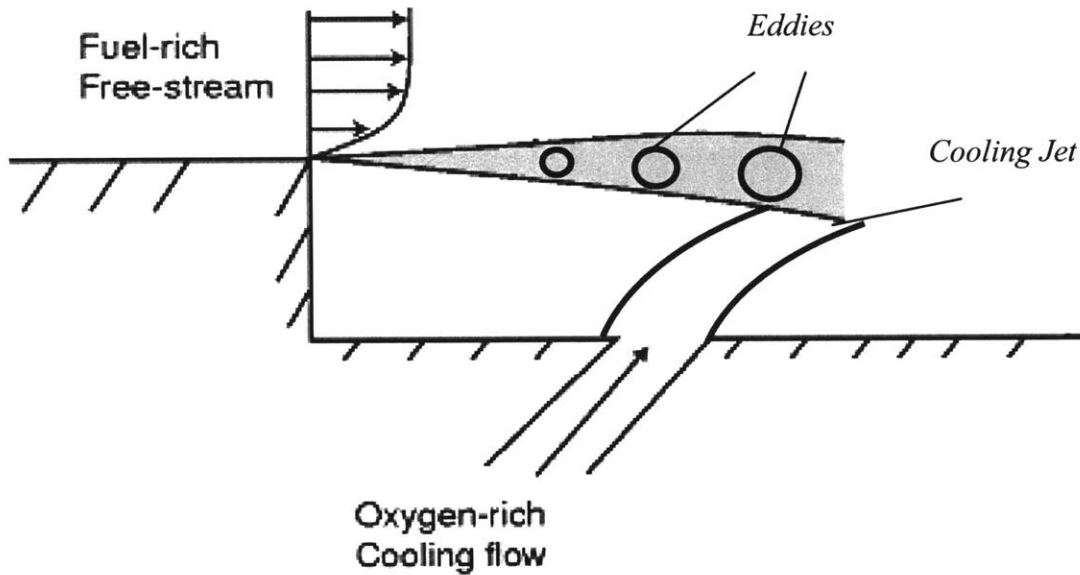
Figure 5-3: Cooling jet interaction with mixing layer eddies

Assuming that the largest eddies dominate momentum flux in the mixing layer, the order of magnitude for an upper bound for the cooling jet momentum blowing ratio was estimated as follows. If the vertical momentum of the cooling jet is of the same order than the vertical momentum of the largest eddies in the mixing layer, then the cooling jet is assumed to alter the structure of the recirculation zone. Thus, the critical momentum blowing ratio, I^*, can be estimated from a vertical momentum balance,

$$u_{y,jet} \dot{m}_{jet} \sim u_{y,eddy} \dot{m}_{eddy}.$$

5-1

Assuming that the eddies are convected along the diving line between the recirculation zone and the mixing layer with a horizontal speed of half of the freestream velocity, the critical momentum blowing ratio is found to be of the order

$$ I^* \sim \left(\frac{h_{eddy}}{d_{jet}} \right) \left(\frac{\tan\theta}{\cos\theta} \right) \left(\frac{1}{\pi \sin\alpha} \right). \qquad \text{5-2} $$

As the diameter of the jet or its injection angle increases, then I^* increases and a cooling jet of fixed blowing ratio is less likely to penetrate through the recirculation zone. If I is much less than I^*, then the cooling jet likely has minimal impact on the flow structure within the recirculation zone. It is important to note that equation 5-2 is merely an order of magnitude estimate and should not be taken as an exact value, because shear and pressure effects on the momentum of the jet and eddy were neglected.

Using the eddy size data from Harinaldi, Ueda, and Mizomoto [7], the critical momentum blowing ratio for the step configuration tested in chapter four was estimated to be 0.84. Momentum blowing ratios for the $B = 0.5$ test runs ranged from 0.05 to 0.07, and for the $B = 2.0$ test runs the I values ranged from 0.7 to 1. These values suggest that the cooling jet does not pierce the recirculation zone in lower mass blowing ratio tests and that the cooling jet could pierce the recirculation zone in the higher mass blowing ratio tests. Exactly what effects the cooling jet had on the flow structure of the recirculation zone for all of the test runs, however, remain unknown.

5.2 Chapter Summary

This chapter compared the values of the scaled heat flux predicted by the reduced-order mixer/PSR model to the values measured during the reacting film-cooled backward-facing step experiments. Due to the discrepancies between predicted and measured scaled heat flux values, it was postulated that the analytical model does not assume the correct recirculation zone flow

structure for high blowing ratio cases. A critical value for the momentum blowing ratio, I^*, was proposed to set a bound for the upper limit of I that does not alter the flow structure of the recirculation zone. Comparison of the momentum blowing ratio values for the test runs of chapter four with the predicted $I^* = 0.84$ showed that the cooling jet in the lower mass blowing ratio ($B = 0.5$) tests likely did not pierce the recirculation zone.

Chapter 6

6 Summary

This chapter summarizes the research efforts presented in this thesis, reviews the research contributions, and outlines recommendations for future work.

6.1 Summary of Research

Heat flux augmentation due to near wall reactions behind film-cooled backward-facing steps was investigated. Due to the high fluid residence times that characterize the recirculation zone downstream of a backward-facing step, chemical reactions can be sustained over a wide range of non-dimensional conditions.

A set of non-dimensional parameters governing reacting heat transfer behind film cooled backward-facing steps was presented. A subset of this parameter set was studied with both a reduced-order analytical model and reacting film-cooled heat transfer experiments.

The analytical model developed was a combination of an ideal mixer and perfectly-stirred reactor in series. The mass flows entrained from the mixing layer and injected by the cooling jet were assumed to mix quickly enough within the recirculation zone to maintain a uniform spatial composition throughout the recirculation zone. Scaled heat flux values of 20-30% were predicted for realistic values of mass blowing ratio, Damköhler number, and heat release potential.

Reacting film-cooled backward-facing step heat transfer experiments were also used to study how each independent member of the governing subset of parameters affects the scaled heat flux. Experiments performed in the MIT Gas Turbine Lab shock tunnel facility showed that scaled heat flux values of up to 75% were measured for similar non-dimensional conditions studied with the analytical model.

The large discrepancy between the predictions of the model and the experimentally measured results could be because the flow structure of the

experimental cases was not consistent with the fundamental assumption of the model. A critical momentum blowing ratio, Γ, suggests that the high mass blowing ratio experimental cases did have altered recirculation zone flow structures. The recirculation zone could have been split in two by the cooling jet, with the upstream smaller zone acting to change the upstream thermodynamic and fluid dynamic boundary conditions of the cooling jet. Three-dimensional flow effects that result from the discrete cooling jet injection could induce the entrainment of gases from the upstream recirculation zone to the flow zone downstream of the cooling jet. These flow effects would not only alter the recirculation zone flow structure and thus violate a fundamental assumption of the model, but could also act as a mechanism by which hot gases from a reacting upstream recirculation zone are continually supplied to the flow zone downstream of the cooling jet. This could explain why higher scaled heat flux values were measured in the experiments than were predicted for similar non-dimensional conditions with the model.

Another possible explanation for the discrepancy between the model predictions and the experimental measurements is the uncertainty associated with the convective heat transfer coefficient. Due to a lack of published data for convection coefficients downstream of film-cooled backward-facing steps, the convection coefficient was taken from [4] with an uncertainty of 10%. This uncertainty was to account for possible differences in the convection coefficient due to the presence of the film cooling jet. As seen in chapter four, this uncertainty propagates and results in a wide error band on the values of scaled heat flux. While this cannot completely account for the discrepancy between the model predictions and the experimental measurements, it does emphasize the need for better convection coefficient models in future work.

6.2 Overview of Research Contributions

This section lists the most significant research contributions of the present work.

- A set of non-dimensional parameters that govern film-cooled reacting backward-facing step heat transfer was developed. The complete parameter set is the superposition of three previously proposed parameter sets governing different aspects of step flow or film-cooled reaction heat transfer. A smaller set of the complete parameter set was derived for study with an analytical model and reactive heat transfer experiment.

- A reduced-order mixer/PSR analytical model was developed. Assuming the flow structure within the recirculation zone was unaffected by the film-cooling jet and that the recirculation zone was "well mixed", scaled heat flux can be predicted for any fluid dynamic, thermodynamic, or geometric conditions.

- Using the mixer/PSR model developed, the effects of step height on scaled heat flux were predicted. For any given values of the governing non-dimensional parameters, the minimum step height required to sustain combustion within the recirculation zone can be predicted.

- The profile of scaled heat flux augmentation downstream of the step face was measured in reacting heat transfer experiments. These profiles were shown for a variety of non-dimensional conditions in chapter four. Similarity in the downstream profile of the $B = 0.5$ step case and the $B = 2.0$ flat plate case suggested that similar heat transfer mechanisms were present.

6.3 Recommendation for Future Work

The following list of actions is recommended for further study of the heat transfer behind film cooled backward-facing steps.

- Perform additional experiments on different step heights to measure the heat flux behind more step configurations.

- Develop a model for the convective heat transfer coefficient behind film-cooled backward-facing steps.

- Complete a computational study with chemical reactions to study:

85

- o the spatial characteristics of reactions behind the step.

- o the flow structure of the recirculation zone with cooling jets present.

- o the effects of additional cooling hole geometries on scaled heat flux.

- Alter the reduced-order model to more accurately represent the physics present in the higher fidelity computational model.

Bibliography

[1] Lukachko, S., Kirk, D., and Waitz, I., "Turbine Durability Impacts of High Fuel-Air Ratio Combustors Part 1: Potential for Intra-Turbine Oxidation of Partially Reacted Fuel," *Proceedings of ASME Turbo Expo 2002*, GT-2002-30077.

[2] Kirk, D., 2002, *Near-Wall Reaction Effects on Film-Cooled Surface Heat Transfer*, Ph.D. thesis, Department of Aeronautics and Astronautics, Massachusetts Institute of Technology.

[3] Adams, E., Johnston, J., and Eaton, J., *Experiments on the Structure of Turbulent Reattaching Flow*, Report MD-43, Department of Mechanical Engineering, Stanford University.

[4] Aung, W., and Goldstein, R., "Heat Transfer in Turbulent Separated Flow Downstream of a Rearward-Facing Step," *Israel Journal of Technology*, Vol. 10, pp. 35-41.

[5] Seban, R., Emery, A., and Levy, A., "Heat Transfer to Separated and Reattached Subsonic Turbulent Flows Obtained Downstream of a Surface Step," *Journal of Aeronautical Sciences*, Vol. 26, pp. 809-814.

[6] Vogel, J., and Eaton, J., "Combined Heat Transfer and Fluid Dynamic Measurements Downstream of a Backward-Facing Step," *ASME Journal of Heat Transfer*, Vol. 107, pp. 922-929.

[7] Harinaldi, Ueda, T., and Mizomoto, M., "Effect of slot gas injection to the flow field and coherent structure characteristics of a backstep flow," *International Journal of Heat and Mass Transfer*, Vol. 44, pp. 2711-2726.

[8] Zukoski, E., and Marble, F., "Experiments Concerning the Mechanism of Flame Blowoff from Bluff Bodies," *Proceedings of the Gas Dynamics Symposium on Aerothermochemistry*, Northwestern University Press, Evanston, Ill., 1955.

[9] Bradshaw, P., and Wong, F., "The Reattachment and Relaxation of a Turbulent Shear Layer," *Journal of Fluid Mechanics*, Vol. 152, pp. 113-135.

[10] Coates, C., and Richardson, A., "Nonpremixed Combustion in Turbulent Mixing Layers Part 1: Flame Characteristics," *Combustion and Flame*, Vol. 122, pp. 253-270.

[11] Underwood, D., 1999, *Primary Zone Modeling for Gas Turbine Combustors*, Sc.D. thesis, Department of Aeronautics and Astronautics, Massachusetts Institute of Technology.

[12] Hermanson, J., and Dimotakis, P., "Effects of Heat Release in a Turbulent, Reattaching Shear Layer," *Journal of Fluid Mechanics*, Vol. 199, pp. 333-375.

[13] Chapman, D., Kuehn, D., and Larson, H., *Investigation of Separated Flows in Supersonic and Subsonic Streams with Emphasis on the Effect of Transition*, NACA Report 1356.

[14] Eaton, J., and Johnston, J., *Turbulent Flow Reattachment: An Experimental Study of the Flow and Structure behind a Backward-Facing Step*, Report MD-39, Department of Mechanical Engineering, Stanford University.

[15] Kerwin, J., 1996, *Design of a shock tube for jet noise research*, Masters thesis, Department of Aeronautics and Astronautics, Massachusetts Institute of Technology.

[16] Vidal, R.J., "Model Instrumentation Techniques for Heat Transfer and Force Measurements in a Hypersonic Shock Tunnel." Cornell Aeronautical Laboratory, Inc. Contract No. AF33(616)-2387, Report No. AD-917-A-1. February 1956.

Appendix A-Complete Test Listing

Table A-1 contains a complete list of all experimental runs. *Step* refers to the 10 mm step attachment piece described in chapter four and shown in detail in appendix B.

Table A-1: Complete list of test runs

Test #	Test Piece	Da	B	I	H*
T002s	plate	2.50	0	0	0
T003s	plate	6.84	0.5	0.047	0.30
T004s	plate	11.25	2.0	0.704	0.25
T005s	plate	9.10	0.5	0.045	0.27
T006s	plate	2.86	0.5	0.054	0.30
T007s	step	17.14	0	0	0
T008s	step	12.91	0.5	0.049	0.32
T009s	step	14.51	0.5	0.048	0.24
T010s	step	8.09	2.0	0.842	0.39
T011s	step	1.99	0.5	0.062	0.53
T012s	step	0.05	0.5	0.089	0.87
T013s	step	8.80	0.5	0.052	0.28
T014s	step	6.36	0.5	0.054	0.41
T015s	step	1.06	0.5	0.066	0.36
T016s	step	17.59	2.0	0.742	0.18
T017s	step	0.96	2.0	1.074	0.60

Appendix B-Experimental Step Piece Drawing

Figure B-1 shows the fabrication drawing for the step attachment used in the experiments. All dimensions listed are in inches.
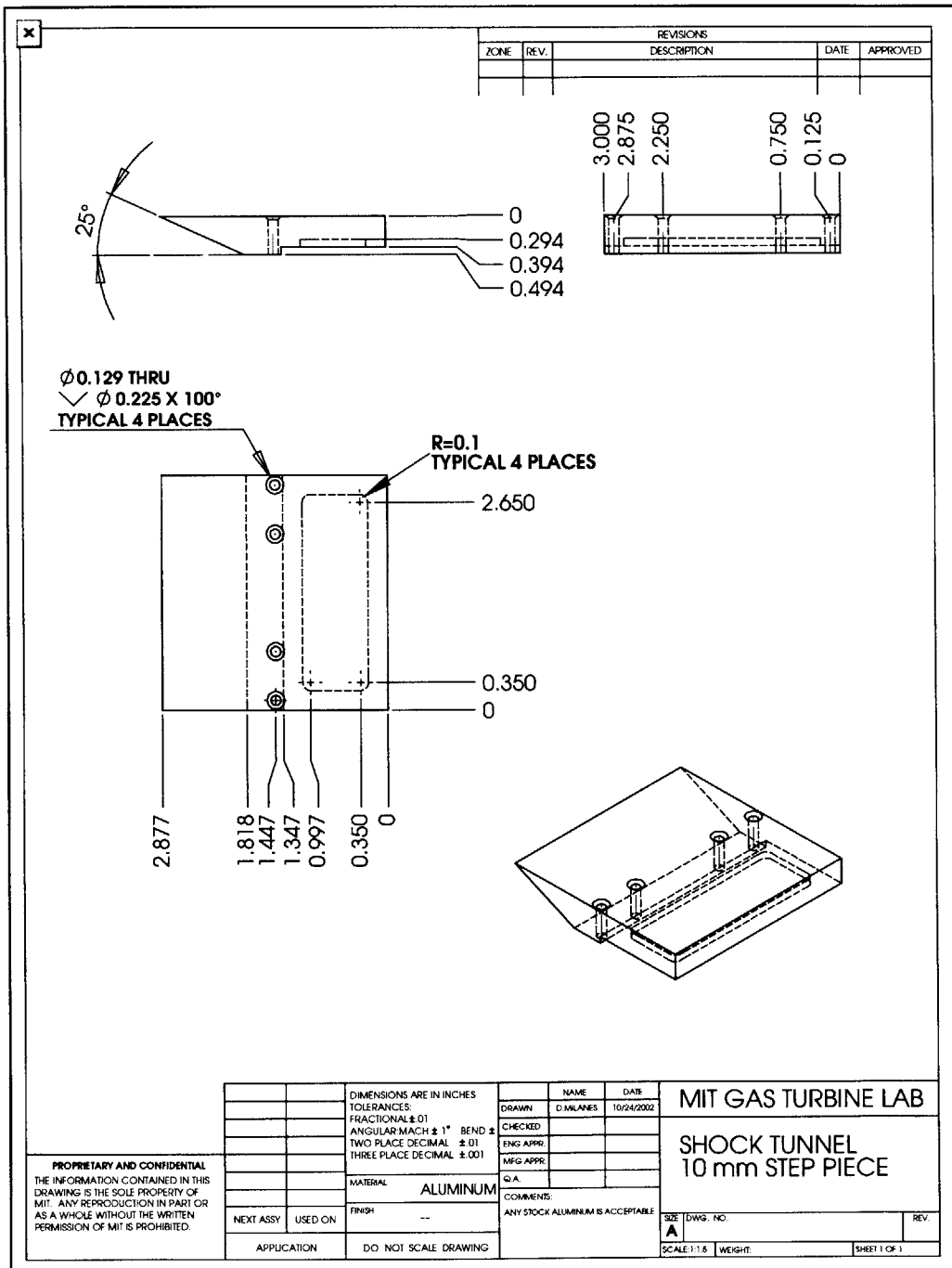

Figure B-1: Shop drawing of experimental step piece

5000
3)